The zebrafish mutant *dreammist* implicates sodium homeostasis in sleep regulation

Ida L. Barlow[1,2], Eirinn Mackay[1,3], Emily Wheater[1,4], Aimee Goel[1], Sumi Lim[1], Steve Zimmerman[5], Ian Woods[6], David A. Prober[7], and Jason Rihel[1,*]

[1] Department of Cell and Developmental Biology, University College London, UK;

[2] Current address: MRC London Institute for Medical Sciences, Imperial College London, UK

[3] Current address: Sainsbury Wellcome Centre for Neural Circuits and Behaviour, University College London, UK

[4] Current address: MRC centre for Reproductive Health, University of Edinburgh, UK

[5] Department of Molecular and Cellular Biology, Harvard University, USA

[6] Ithaca College, New York, USA

[7] Division of Biology and Biological Engineering, California Institute of Technology, Pasadena, USA

* Lead author: Jason Rihel j.rihel@ucl.ac.uk

Significance statement: Sleep is an essential behavioral state, but the genes that regulate sleep and wake states are still being uncovered. A viral insertion screen in zebrafish identified a novel sleep mutant called *dreammist*, in which a small, highly-conserved transmembrane protein is disrupted. The discovery of *dreammist* highlights the importance of a class of small transmembrane-protein modulators of the sodium pump in setting appropriate sleep duration.

Abstract

Sleep is a nearly universal feature of animal behaviour, yet many of the molecular, genetic, and neuronal substrates that orchestrate sleep/wake transitions lie undiscovered. Employing a viral insertion sleep screen in larval zebrafish, we identified a novel gene, *dreammist* (*dmist*), whose loss results in behavioural hyperactivity and reduced sleep at night. The neuronally expressed *dmist* gene is conserved across vertebrates and encodes a small single-pass transmembrane protein that is structurally similar to the Na^+,K^+-ATPase regulator, FXYD1/Phospholemman. Disruption of either *fxyd1* or *atp1a3a*, a Na^+,K^+-ATPase alpha-3 subunit associated with several heritable movement disorders in humans, led to decreased night-time sleep. Since *atpa1a3a* and *dmist* mutants have elevated intracellular Na^+ levels and non-additive effects on sleep amount at night, we propose that Dmist-dependent enhancement of Na^+ pump function modulates neuronal excitability to maintain normal sleep behaviour.

Introduction

The ability of animals to switch between behaviourally alert and quiescent states is conserved across the animal kingdom (Cirelli, 2009; Joiner, 2016). Fundamental processes that govern the regulation of sleep-like states are shared across species, such as the roles of circadian and homeostatic cues in regulating the time and amount of sleep, stereotyped postures, heightened arousal thresholds, and the rapid reversibility to a more alert state (Joiner, 2016). The near ubiquity of sleep implies that it serves ancient functions and is subject to conserved regulatory processes. However, many key molecular components that modulate sleep and wake states remain undiscovered.

Over the past two decades, investigations into sleep and arousal states of genetically tractable model organisms, such as *Drosophila melanogaster*, *C. elegans*, and *Danio rerio* (zebrafish) have uncovered novel molecular and neuronal components of sleep regulation

through gain- and loss-of-function genetic screens (reviewed in Barlow and Rihel, 2017; Sehgal and Mignot, 2011). The power of screening approaches is perhaps best exemplified by the first forward genetic sleep screen, which identified the potassium channel *shaker* as a critical sleep regulator in *Drosophila* (Cirelli et al., 2005). This result continues to have a lasting impact on the field, as not only did subsequent sleep screening efforts uncover the novel Shaker regulator *sleepless*, (Koh et al., 2009), but investigations into Shaker's beta subunit Hyperkinetic ultimately revealed a critical role for this redox sensor linking metabolic function to sleep (Bushey et al., 2007; Kempf et al., 2019).

Disparate screening strategies across model organisms continue to unveil novel sleep modulators in both invertebrate and vertebrate model systems. For example, the roles of RFamide receptor DMSR-1 in stress-induced sleep in *C. elegans* (Iannacone et al., 2017) and SIK3 kinase in modulating sleep homeostasis in mice (Funato et al., 2016) were identified in genetic screens. Moreover, a gain of function screening strategy in *Drosophila* revealed the novel sleep and immune regulator, *nemuri* (Toda et al., 2019), and a zebrafish overexpression screen uncovered the secreted neuropeptides neuromedin U and neuropeptide Y, which decrease and increase sleep, respectively (Chiu et al., 2016; Singh et al., 2017). The success of screening strategies in revealing novel sleep-wake regulatory genes suggests that more sleep signals likely remain to be discovered.

One of the lessons from these genetic screens is that many of the uncovered genes play conserved roles across species. For example, Shaker also regulates mammalian sleep (Douglas et al., 2007) and RFamides induce sleep in worms, flies, and vertebrates (Lee et al., 2017; Lenz et al., 2015). Nevertheless, not every invertebrate sleep-regulatory gene has a clear vertebrate homolog, while some known human sleep/wake regulators, such as the narcolepsy-associated neuropeptide hypocretin/orexin (Chemelli et al., 1999; Lin et al., 1999; Peyron et al., 2000; Sakurai, 2013), lack invertebrate orthologs. Therefore, genetic sleep

74 screens in vertebrates are likely to provide added value in uncovering additional regulatory
75 components required to control the initiation and amount of sleep in humans.

76 While sleep screening in mammals is feasible (Funato et al., 2016), it remains an expensive
77 and technically challenging endeavour. With its genetic tractability, availability of high-
78 throughput sleep assays (Rihel and Schier, 2013), and conserved sleep genetics, such as the
79 hypocretin, melatonin, locus coeruleus, and raphe systems (Gandhi et al., 2015; Singh et al.,
80 2015; Oikonomou et al., 2019; Prober et al., 2006), the larval zebrafish is an attractive
81 vertebrate system for sleep screens. We took advantage of a collection of zebrafish lines that
82 harbour viral-insertions in >3500 genes (Varshney et al., 2013) to perform a targeted genetic
83 screen. We identified a short-sleeping mutant, *dreammist*, with a disrupted novel, highly
84 conserved vertebrate gene that encodes a small single pass transmembrane protein.
85 Sequence and structural homology to the Na^+/K^+ pump regulator FXYD1/Phospholemman
86 suggests that Dreammist is a neuronal-expressed member of a class of sodium pump
87 modulators that is important for regulating sleep-wake behaviour.

88 **RESULTS**

89 **Reverse genetic screen identifies *dreammist,* a mutant with decreased sleep**

90 We used the 'Zenemark' viral-insertion based zebrafish gene knock-out resource (Varshney
91 et al., 2013) to perform a reverse genetic screen to identify novel vertebrate sleep genes. This
92 screening strategy offers several advantages compared to traditional chemical mutagenesis-
93 based forward genetic screening approaches. First, unlike chemical mutagenesis, which
94 introduces mutations randomly, viral insertions tend to target the 5' end of genes, typically
95 causing genetic loss of function (Sivasubbu et al., 2007). Second, because the virus sequence
96 is known, it is straightforward to map and identify the causative gene in mutant animals. Finally,
97 since viral insertions in the Zenemark collection are already mapped and sequenced, animals
98 harbouring insertions within specific gene classes can be selected for testing (Figure S1A).
99 This allowed us to prioritise screening of genes encoding protein classes that are often linked
100 to behaviour, such as G-protein coupled receptors, neuropeptide ligands, ion channels, and
101 transporters (Supplemental Data 1).

102 For screening, we identified zebrafish sperm samples from the Zenemark collection
103 (Varshney et al., 2013) that harboured viral insertions in genes of interest and used these
104 samples for *in vitro* fertilization and the establishment of F2 families. For each viral insertion
105 line, clutches from heterozygous F2 in-crosses were raised to 5 days post-fertilisation (dpf) and
106 tracked using videography (Figure S1A) to quantify the number and duration of sleep bouts
107 (defined in zebrafish larvae as inactivity lasting 1 minute or longer; Prober et al., 2006) and
108 waking activity (time spent moving per active bout) over 48 hours. The genotypes of individual
109 larvae were determined by PCR after behavioural tracking, with each larva assigned as wild
110 type, heterozygous, or homozygous for a given viral insertion to assess the effect of genotype
111 on sleep/wake behaviour. While most screened lines had minimal effects on sleep-wake
112 behavioural parameters (Figure S1B-S1C), one homozygous viral insertion line, *10543/10543,*

113 had a reduction in daytime sleep (Figure S1B) and an increase in daytime waking activity
114 (Figure S1C) relative to their wild type sibling controls. We re-named this *10543* viral insertion
115 line *dreammist* (*dmist*).

116 In follow-up studies, we observed that animals homozygous for the viral insertion at this
117 locus (*dmist*$^{vir/vir}$) showed a prominent decrease in sleep during the day and a trend to sleep
118 less at night compared to their wild-type siblings (*dmist*$^{+/+}$) (Figure 1A). *dmist* mutants had an
119 almost 50% reduction in the average amount of daytime sleep (Figure 1C) due to a decrease
120 in the number of sleep bouts (Figure 1D), whereas the sleep bout length at night was
121 significantly reduced (Figure 1E). *dmist*$^{vir/vir}$ larvae also exhibited significantly increased
122 daytime waking activity, which is the locomotor activity while awake (Figure 1B, 1F). Because
123 Zenemark lines can contain more than one viral insertion (17.6% of lines have ≥2 insertions;
124 Varshney et al 2013), we outcrossed *dmist*$^{vir/+}$ fish to wild-type fish of the AB-TL background
125 and re-tested *dmist* mutant fish over several generations. Normalising all the behavioural
126 parameters to *dmist*$^{+/+}$ controls with a linear mixed effects (LME) model showed consistent
127 sleep changes in *dmist*$^{vir/vir}$ fish over 5 independent experiments (Figure 1G). The *dmist*$^{vir/vir}$
128 larvae consistently show a more than 50% decrease in sleep during the day due to a significant
129 reduction in the number and duration of sleep bouts, as well as a large increase in waking
130 activity (Figure 1G). The *dmist*$^{vir/vir}$ mutants also had a significant reduction in sleep at night
131 compared to wild type siblings (Figure 1G). These effects on sleep and wakefulness are not
132 due to alterations in circadian rhythms, as behavioural period length in fish that were entrained
133 and then shifted to free-running constant dark conditions was unaffected in *dmist*$^{vir/vir}$ compared
134 to wild-type sibling larvae (Figure S2A-S2C).

135

136 **The *dmist* gene encodes a novel, small transmembrane protein**

137 Having identified a sleep mutant, we next sought to investigate the target gene disrupted by
138 the viral insertion. Line *10543* (*dmist*^{vir}) was initially selected for screening due to a predicted
139 disruption of a gene encoding a serotonin transporter (*slc6a4b*) on chromosome 5. However,
140 mapping of the *dmist* viral insertion site by inverse-PCR and sequencing revealed that the virus
141 was instead inserted into the intron of a small two-exon gene annotated in the Zv6 genome
142 assembly as a long intergenic non-coding RNA (lincRNA; gene transcript
143 ENSDART00000148146, gene name *si:dkey234h16.7*), which lies approximately 6 kilobases
144 (kb) downstream of the *slc6a4b* gene in zebrafish. At least part of this region is syntenic across
145 vertebrates, with a small two-exon gene identified adjacent to the genes *ankrd13a* and *GIT* in
146 several vertebrates, including human and mouse (Figure 2A). Amplifying both 5' and 3' ends
147 of zebrafish *si:dkey234h16.7* and mouse E13.5 *1500011B03-001* transcripts with Rapid
148 Amplification of cDNA ends (RACE) confirmed the annotated zebrafish and mouse transcripts
149 and identified two variants with 3' untranslated regions (3'UTR) of different lengths in zebrafish
150 (Figure S3B). To test whether the viral insertion in *dmist*$^{vir/vir}$ disrupts expression of
151 *si:dkey234h16.7* or neighbouring genes, we performed quantitative analysis of gene transcript
152 levels in wild type and mutant *dmist* larvae by RT-qPCR. This revealed that the *dmist* viral
153 insertion caused a more than 70% reduction in the expression of *si:dkey234h16.7* while the
154 expression of the most proximal 5' or 3' flanking genes, *slc6a4b_Dr* and *ankrd13a_Dr*, were
155 unaffected (Figure 2B and S3A). Since this reduced expression is most consistent with
156 *si:dkey234h16.7* being the causal lesion of the *dmist* mutant sleep phenotype, we renamed
157 this gene *dreammist* (*dmist*).

158 Computational predictions indicated that the *dmist* transcripts contain a small open reading
159 frame (ORF) encoding a protein of 70 amino acids (aa) (Figure 2C, Figure S3B). Querying the
160 human and vertebrate protein databases by BLASTp using the C-terminal protein sequence of
161 Dmist identified orthologs in most vertebrate clades, including other species of teleost fish,

162 birds, amphibians, and mammals (Figure 2A, C). All identified orthologs encoded predicted
163 proteins with an N-terminal signal peptide sequence and a C-terminal transmembrane domain
164 (Figure 2C). The peptide sequence identity across orthologs ranged from 38 to 84%, with three
165 peptide motifs (QNLV, CVYKP, RRR) showing high conservation across all vertebrates, and
166 high similarity for many additional residues (Figure 2C, Figure S3D). Additional searches by
167 tBLASTn failed to identify any non-vertebrate *dmist* orthologs. In summary, we found that the
168 *dreammist* gene, the expression of which is disrupted in *dmist*$^{vir/vir}$ fish with sleep phenotypes,
169 encodes a protein of uncharacterized function that is highly conserved across vertebrates at
170 both the genomic and molecular levels.

171

172 **Genetic molecular analysis of *dmist* expression in zebrafish and mouse**

173 Because the viral insertion disrupts *dmist* throughout the animal's lifetime, we examined
174 both the developmental and spatial expression of *dmist* to assess when and where its function
175 may be required for normal sleep. Using the full-length transcript as a probe (Figure S3B), we
176 performed *in situ* hybridization across embryonic and larval zebrafish development. Maternally
177 deposited *dmist* was detected in early embryos (2-cell stage) prior to the maternal to zygotic
178 transition (Giraldez et al., 2006) (Figure 2D). Consistent with maternal deposition of *dmist*
179 transcripts, inspection of the 3' end of the *dmist* gene revealed a cytoplasmic polyadenylation
180 element ('TTTTTTAT'; Supplemental Information 2) that is required for zygotic translation of
181 maternal transcripts (Villalba et al., 2011). At 24 hpf, transcripts were detected in regions that
182 form the embryonic brain, such as ventral telencephalon, diencephalon and cerebellum, and
183 in the developing eye (Figure 2D, S3C). By 5 dpf, *dmist* transcripts were detected throughout
184 the brain (Figure 2D). To test whether *dmist* transcripts are under circadian regulation, we
185 performed RT-qPCR in fish that were entrained and then shifted to free-running constant dark
186 conditions. In contrast with the robust 24-hr rhythmic transcription of the circadian clock gene

187 *per1*, we did not detect any changes in *dmist* expression throughout the 24 hour circadian cycle
188 (Figure S2D).

189 Consistent with brain expression in larval zebrafish, we identified the expression of
190 *Dmist_Mm* in a published RNAseq dataset of six isolated cell types from mouse cortex (Zhang
191 et al., 2014). We confirmed that *Dmist_Mm* is specifically enriched in neurons by hierarchical
192 clustering of all 16,991 expressed transcripts across all six cells types, which demonstrated
193 that *Dmist_Mm* co-clusters with neuronal genes (Figure S3E). Pearson correlation of
194 *Dmist_Mm* with canonical markers for the six cell types showed that *Dmist_Mm* expression is
195 highly correlated with other neuronal genes but not genes associated with microglia,
196 oligodendrocytes, or endothelia. This result indicates that *dmist* is specifically expressed in
197 neurons in both zebrafish and mouse (Figure S3F).

198

199 **Dmist localises to the plasma membrane**

200 Although the *dmist* gene encodes a conserved ORF with a predicted signal peptide
201 sequence and transmembrane domain (Figure 2C; Figure S3G-I), we wanted to confirm this
202 small peptide can localise to the membrane and if so, on which cellular compartments. To test
203 these computational predictions, we transiently co-expressed GFP-tagged Dmist (C-terminal
204 fusion) with a marker for the plasma membrane (myr-Cherry) in zebrafish embryos. Imaging at
205 90% epiboly revealed Dmist-GFP localised to the plasma membrane (Figure 2E). Conversely,
206 introducing a point mutation into Dmist's signal peptide cleavage site (DmistA22W-GFP)
207 prevented Dmist from trafficking to the plasma membrane, with likely retention in the
208 endoplasmic reticulum (Figure 2F). Together, these data indicate that Dmist localises to the
209 plasma membrane despite its small size, as computationally predicted.

210

211 **CRISPR/Cas9 generated *dmist^{i8}* mutant exhibits decreased night-time sleep**

212 *dmist* expression was reduced by 70% in the viral insertion line, suggesting that *dmist*^{vir} is a
213 hypomorphic allele. To confirm that the sleep phenotypes observed in *dmist*$^{vir/vir}$ animals are
214 due to the loss of Dmist function, we used CRISPR/Cas9 to create an independent *dmist* loss
215 of function allele. We generated a zebrafish line in which the *dmist* gene contains an 8 bp
216 insertion that causes a frameshift and early stop codon (*dmist*^{i8}, Figure 3A). The *dmist*^{i8} allele
217 is predicted to encode a truncated protein lacking the complete signal peptide sequence and
218 transmembrane domain (Figure 3B), indicating this is likely a null allele. RT-qPCR showed that
219 *dmist* transcript levels were 60% lower in *dmist*$^{i8/i8}$ fish compared to wild type siblings,
220 consistent with nonsense-mediated decay (Figure S4A, B).

221 We next assessed the sleep and activity patterns of *dmist*$^{i8/i8}$ fish. As seen in exemplar
222 individual tracking experiments, *dmist*$^{i8/i8}$ larvae sleep less at night due to fewer sleep bouts
223 and also show an increase in waking activity relative to wild type and heterozygous mutant
224 siblings (Figure 3C-H). This significant night-time reduction in sleep and increase in
225 hyperactivity is also apparent when combining 5 independent experiments with an LME model
226 to normalize behaviour across datasets (Figure 3I). Although *dmist*$^{vir/vir}$ larvae also sleep less
227 at night (Figure 1G), the large day-time reduction in sleep observed in *dmist*$^{vir/vir}$ larvae is absent
228 in *dmist*$^{i8/i8}$ animals, perhaps due to differences in genetic background that affect behaviour.
229 Because the *dmist*^{vir} is likely a hypomorphic allele, we focused subsequent experiments on the
230 CRISPR-generated *dmist*$^{i8/i8}$ larvae.

231 To test whether the increased night-time activity of *dmist*$^{i8/i8}$ mutants persists in older
232 animals, we raised *dmist*$^{i8/i8}$ mutants with their heterozygous and wild type siblings to adulthood
233 in the same tank and tracked individual behaviour for several days on a 14:10 light:dark cycle.
234 As in larval stages, *dmist*$^{i8/i8}$ adults were hyperactive relative to both *dmist*$^{i8/+}$ and *dmist*$^{+/+}$
235 siblings, maintaining a higher mean speed at night (Figure 3J-L). This suggests that either
236 Dmist affects a sleep/wake regulatory circuit during development that is permanently altered in

237 *dmist* mutants, or that Dmist is continuously required to maintain normal levels of night-time
238 locomotor activity.

239

240 **Dmist is distantly related to the Na^+/K^+ pump regulator Fxyd1 (Phospholemman)**

241 Because Dmist is a small, single pass transmembrane domain protein without any clear
242 functional motifs that has not been functionally characterized in any species, we searched for
243 similar peptides that might provide clues for how Dmist regulates behaviour. Using the multiple
244 sequence alignment tool MAFFT to align the zebrafish, mouse, and human Dmist peptides
245 (Katoh and Toh, 2010) and seeding a JackHMMR iterative search of the Uniprot database
246 (Johnson et al., 2010) found distant homology between Dmist and Fxyd1/Phospholemman
247 (Figure 4A), a small transmembrane domain peptide that regulates ion channels and pumps,
248 including the Na^+,K^+-ATPase pump (Crambert et al., 2002). Dmist and Fxyd1 share 27-34%
249 amino acid homology, including an RRR motif at the C-terminal end, although Dmist lacks a
250 canonical FXYD sequence (Figure 4A). In addition, computational predictions using the
251 AlphaFold protein structure database revealed structural similarities between Dmist and Fxyd1
252 (Jumper et al., 2021), suggesting that Dmist may belong to a class of small, single pass
253 transmembrane ion pump regulators.

254 Using *In situ* hybridisation, we found that *fxyd1* is expressed in cells along the brain ventricle
255 and choroid plexus (Figure 4C) in contrast to the neuronal expression of *dmist* (Figure 2D).
256 Despite these different expression patterns, based on their sequence similarity we reasoned
257 that Fxyd1 and Dmist may regulate the same molecular processes that are involved in sleep.
258 To test this hypothesis, we used CRISPR/Cas9 to generate a 28 bp deletion in the third exon
259 of the zebrafish *fxyd1* gene, causing a frameshift that is predicted to encode a truncated protein
260 that lacks the FXYD, transmembrane, and C-terminal domains (Figure 4B). Contrary to a
261 previous report based on morpholino knockdown (Chang et al., 2012), $fxyd1^{\Delta 28/\Delta 28}$ larvae were

262 viable with no detectable defect in inflation of the brain ventricles. We therefore tested *fxyd1*
263 mutant larvae for sleep phenotypes. Like *dmist* mutants, *fxyd1*$^{\Delta 28/\Delta 28}$ larvae slept less at night
264 (Figure 4D-F). Interestingly, this sleep loss is mainly due to shorter sleep bouts (Figure 4F),
265 indicating that *fxyd1* mutants initiate sleep normally but do not properly maintain it, unlike *dmist*
266 mutants, which initiate fewer night-time sleep bouts, although in both cases there is
267 consolidation of the wake state at night (Figure 3I, 4F). Thus, despite the non-neuronal
268 expression of *fxyd1* in the brain, mutation of the gene most closely related to *dmist* results in a
269 similar sleep phenotype.

270

271 **The brain-wide Na^+/K^+ pump alpha subunit Atp1a3a regulates sleep at night**

272 Given the similarity between Dmist and Fxyd1 and their effects on night-time sleep, we
273 hypothesized that mutations in Na^+/K^+ pump subunits known to interact with Fxyd1 might also
274 affect sleep. Consistent with this hypothesis, a low dose of the Na^+/K^+ pump inhibitor, ouabain,
275 reduced night-time sleep in dose-response studies (Figure S5A). When applied in the late
276 afternoon of 6 dpf, 1 μM ouabain decreased subsequent night-time sleep by 16.5% relative to
277 controls, an effect size consistent with those observed in *dmist* mutants (Figure 6A, C). Night-
278 time waking activity was also significantly increased after low-dose ouabain exposure (Figure
279 6B, D). Ouabain binds to specific sites within the first extracellular domain of Na^+/K^+ pump
280 alpha subunits (Price and Lingrel, 1988), and species-specific changes to these sites confers
281 species-specific ouabain resistance, as in the case of two naturally occurring amino acid
282 substitutions present in the Atp1a1 subunit of mice (Dostanic et al., 2004). Alignment of the
283 ouabain sensitive region of zebrafish and mouse Na^+/K^+ pump alpha subunits revealed that
284 zebrafish Atp1a1a lacks the conserved Glutamine at position 121 (Figure 5E), suggesting that
285 one of the other subunits with conserved ouabain-binding sites is responsible for the low dose
286 ouabain sleep effects. We focused on the Na^+/K^+ pump alpha-3 subunit (Atp1a3), as this has

287 been shown to directly interact with Fxyd1 in mammalian brain tissue (Feschenko et al., 2003).
288 Murine *Dmist* expression also correlates well with the *Atp1a3* distribution across 5 brain cell
289 types in mouse (Pearson correlation coefficient = 0.63), which has the strongest correlation
290 score with neuronal markers (Figure S5B compared to Figure S3F). In contrast, zebrafish
291 *atp1a2a* is reportedly expressed in muscle at larval stages, while *atp1a1b* is confined to cells
292 along the ventricle (Thisse et al., 2001).

293 Zebrafish have two Atp1a3 paralogs, *atp1a3a* and *atp1a3b*. Similar to *dmist*, *atp1a3a* is
294 widely expressed in the larval zebrafish brain (Figure 5F, compare to Figure 2D). While *atp1a3b*
295 is also expressed in the zebrafish brain, its expression is more limited to regions of the midbrain
296 and hindbrain (Figure S5C). To test whether these genes are involved in regulating zebrafish
297 sleep, we used CRISPR/Cas9 to isolate an allele of *atp1a3a* containing a 19 bp deletion and
298 an allele of *atp1a3b* containing a 14 bp deletion. Both mutations are predicted to generate null
299 alleles due to deletion of the start codon (Figure 5G, S5D). Both *atp1a3a*$^{\Delta 19/\Delta 19}$ and
300 *atp1a3b*$^{\Delta 14/\Delta 14}$ mutant larvae were healthy and viable through early development, although
301 atp1a3b mutant larvae were not obtained at Mendelian ratios. Contrary to a previous report
302 based on morpholino injections (Doğanli et al., 2013), neither mutant had defects in the inflation
303 of their brain ventricles. Sleep-wake tracking experiments found that *atp1a3b*$^{\Delta 14/\Delta 14}$ mutants
304 were more active during the day with minimal sleep phenotypes (Figure S5E-G). In contrast,
305 mutation of *atp1a3a* resulted in large effects on sleep-wake behaviour. Compared to wild type
306 and heterozygous mutant siblings, *atp1a3a*$^{\Delta 19/\Delta 19}$ animals were hyperactive throughout the day
307 and night and had a large reduction in sleep at night (Figure 5H, I). The night-time sleep
308 reduction was due to a reduction in the length of sleep bouts, as *atp1a3a* mutants even had a
309 small increase in the number of sleep bouts at night (Figure 5J). In conclusion, loss of *atp1a3a*
310 results in sleep loss at night, similar to treatment with the small molecule *ouabain*, and to *dmist*

311 and *fxyd1* mutants. Notably, the *atp1a3a* mutant phenotype is much stronger, as might be
312 expected if Dmist plays a modulatory, and Atp1a3a a more central, role in Na^+/K^+ pump activity.

313

314 **Dmist modulates Na^+/K^+ pump function and neuronal activity-induced sleep**
315 **homeostasis**

316 The similar night-time reduction in sleep in *dmist* and *atp1a3a* mutants, combined with the
317 similarities between Dmist and Fxyd1, suggested that Dmist may regulate the Na^+/K^+ pump.
318 We therefore exposed wild type and mutant larvae to pentylenetetrazol (PTZ), a GABA-
319 receptor antagonist that leads to globally heightened neuronal activity and elevated intracellular
320 sodium levels that must be renormalized by Na^+/K^+ pump activity. Consistent with the
321 hypothesis that Dmist and Atp1a3a subunits are important for a fully functional Na^+/K^+ pump,
322 brains from both *dmist*$^{i8/i8}$ and *atp1a3a*$^{\Delta 19/\Delta 19}$ larvae had elevated intracellular sodium levels
323 after exposure to PTZ (Figure 6A). Thus, neither *dmist* nor *atp1a3a* mutants were able to
324 restore intracellular sodium balance after sustained neuronal activity as quickly as wild type
325 siblings. Consistent with the night-specific alterations in sleep behaviour, we also found that
326 baseline brain Na^+ levels in *dmist* mutants were significantly elevated at night but not during
327 the day (Figure 6B). Collectively, these data are consistent with the hypothesis that night-time
328 sleep duration is affected by changes in Na^+/K^+ pump function and that Dmist is required to
329 maintain this function both at night and after sustained high levels of neuronal activity.

330 We have previously shown in zebrafish that a brief exposure to hyperactivity-inducing drugs
331 such as the epileptogenic PTZ or wake-promoting caffeine induces a dose-dependent increase
332 in homeostatic rebound sleep following drug washout that is phenotypically and mechanistically
333 similar to rebound sleep following physical sleep deprivation (Reichert et al., 2019). Based on
334 their exaggerated intracellular Na^+ levels following exposure to PTZ, we predicted that *dmist*

335 mutants would also have increased rebound sleep in response to heightened neuronal activity.
336 Upon wash-on/wash-off of lower dose (5 mM) PTZ, sleep rebound occurs in approximately
337 50% of wild type larvae (Reichert et al., 2019; Figure 6C, D). In contrast, all *dmist*$^{i8/i8}$ larvae
338 showed increased rebound sleep compared to *dmist*$^{+/+}$ sibling controls (Figure 6C-E). Taken
339 together with the elevated sodium retention experiments, such increases in rebound sleep
340 induced by neuronal activity suggests that *dmist*$^{i8/i8}$ fish more rapidly accumulate sleep
341 pressure in response to heightened neuronal activity.

342 Finally, we predicted that if Dmist is affecting baseline sleep via modulation of Atp1a3a-
343 containing Na^+/K^+ pumps, *dmist*$^{-/-}$; *atp1a3a*$^{-/-}$ double mutants should have a reduction in night-
344 time sleep that is not the sum of effects from either mutant alone. In other words, if Dmist and
345 Atp1a3a are acting in separate pathways, the double mutant would have an additive
346 phenotype, but if Dmist and Atp1a3a act together in the same complex/pathway, the mutant
347 phenotypes should be non-additive. Indeed, *dmist*$^{-/-}$; *atp1a3a*$^{-/-}$ mutants have a sleep reduction
348 similar to that of *atp1a3a*$^{-/-}$ mutants alone, consistent with a non-additive effect (Figure 6F and
349 S6). Similar non-additivity can be also observed in the *dmist*$^{-/-}$; *atp1a3a*$^{+/-}$ animals, which, like
350 *atp1a3a*$^{+/-}$ animals alone, have a milder sleep reduction, indicating that the lack of additivity
351 between dmist and atp1a3a phenotypes is unlikely due to a floor effect, since double
352 homozygous mutants can sleep even less (Figure 6F). This genetic interaction data is
353 consistent with our hypothesis that Atp1a3a and Dmist act in the same pathway—the Na^+/K^+
354 pump-- to influence sleep.

355

356 **DISCUSSION**

357 **Genetic screening discovers *dmist*, a novel sleep-regulatory gene**

358 Using a reverse genetic viral screening strategy, we discovered a short-sleeping mutant,
359 *dmist*, which has a disruption in a previously uncharacterized gene encoding a small

360 transmembrane peptide. Given that the *dmist* mutant appeared within the limited number of 25
361 lines that we screened, it is likely that many other sleep genes are still waiting to be discovered
362 in future screens. In zebrafish, one promising screening strategy will be to employ
363 CRISPR/Cas9 genome editing to systematically target candidate genes. Advances in the
364 efficiency of this technology now makes it feasible to perform a CRISPR "F0 screen" in which
365 the consequences of bi-allelic, gene-specific mutations are rapidly tested in the first generation,
366 with only the most promising lines pursued in germline-transmitted mutant lines (Grunwald et
367 al., 2019; Jao et al., 2013; Kroll et al., 2021; Shah et al., 2015; Shankaran et al., 2017; Wu et
368 al., 2018). CRISPR F0 screens could be scaled to systematically target the large number of
369 candidate sleep-regulatory genes identified through human GWAS studies and sequencing of
370 human patients suffering from insomnia and neuropsychiatric disorders (Allebrandt et al., 2013;
371 Dashti et al., 2019; Jansen et al., 2019; Jones et al., 2019; Lane et al., 2019; Lek et al., 2016;
372 Palagini et al., 2019).

373

374 **Dmist is related to the Na+/K+ pump regulator Fxyd1**

375 The small Dmist transmembrane protein is highly conserved across vertebrates, expressed
376 in neurons, and important for maintaining normal sleep levels. How can such a small, single
377 pass transmembrane protein lacking any clear functional domains modulate the function of
378 neurons and ultimately animal behaviour? The recognition that Dmist has sequence homology
379 (~35% amino acid similarity; a conserved 'RRR' motif in the C-terminus) and structural
380 homology (e.g. signal peptide and single pass transmembrane domains) to the Na^+,K^+-ATPase
381 pump regulator Fxyd1 (Phospholemman) offers some important clues.

382 Fxyd1/Phospholemman is a member of the FXYD protein family, of which there are seven
383 mammalian members (Sweadner and Rael, 2000). Each of the FXYD proteins is small,
384 contains a characteristic FXYD domain, and has a single transmembrane domain. FXYD family

385 members interact with alpha subunits of the Na^+,K^+ ATPase to regulate the function of this
386 pump, with individual family members expressed in different tissues to modulate Na^+,K^+-
387 ATPase activity depending on the physiological needs of the tissue (Geering et al., 2003). In
388 cardiac muscle, FXYD1 is thought to act as a hub through which various signalling cascades,
389 such as PKA, PKC, or nitric oxide, can activate or inhibit Na^+ pump activity (Pavlovic et al.,
390 2013). For example, FXYD1 is critical for mediating the increased Na^+ pump activity observed
391 after β-receptor stimulation via cAMP-PKA signalling (Despa et al., 2008). Much less is known
392 about the role of FXYD1 in non-cardiac tissue, although it is expressed in neurons in the
393 mammalian cerebellum, the choroid plexus, and ependymal cells, where it interacts with all
394 three alpha subunits of the Na^+,K^+ ATPase (Feschenko et al., 2003).

395 In zebrafish, we also found that *fxyd1* is expressed in cells around the ventricles and in the
396 choroid plexus (Figure 4C), in contrast to *dmist* which is expressed in neurons throughout the
397 brain. Despite the different expression patterns, mutation of each gene resulted in a similar
398 reduction of sleep at night. However, unlike *dmist* mutants, which have fewer sleep bouts (i.e.
399 initiate sleep less) and an increase in waking locomotor activity, *fxyd1* mutants have shorter
400 sleep bouts (i.e. cannot maintain sleep) on average and do not have a locomotor activity
401 phenotype. Just as the various FXYD family members modulate the Na^+/K^+ pump in different
402 tissue- and context-specific ways, this phenotypic variation between *fxyd1* and *dmist* mutants
403 could be due to the different *fxyd1* and *dmist* expression patterns, modulation kinetics of
404 pump/channel dynamics, or interaction with different accessory proteins or signal transduction
405 cascades. Nevertheless, the similar timing and magnitude of sleep reduction, combined with
406 the structural similarity of Fxyd1 and Dmist, suggest that they may regulate similar sleep-
407 related processes.

408

409 **Dmist, the sodium pump, and sleep**

410 The similarity between Dmist and FXYD1 led us to directly manipulate the Na^+,K^+ ATPase
411 to test its importance in sleep. The Na^+,K^+-ATPase is the major regulator of intracellular Na^+ in
412 all cells and, by actively exchanging two imported K^+ ions for three exported Na^+ ions, is
413 essential for determining cellular resting membrane potential (reviewed in Clausen et al.,
414 2017). The Na^+,K^+-ATPase consists of a catalytic alpha subunit (4 known isoforms, ATP1A1-
415 4), a supporting beta subunit (3 isoforms, ATP1B1-3), and a regulatory gamma subunit (the
416 FXYD proteins). The alpha1 and alpha3 subunits are the predominant catalytic subunits in
417 neurons (alpha2 is mostly restricted to glia), although the alpha1 subunit is also used
418 ubiquitously in all tissues (McGrail et al., 1991). By mutating zebrafish orthologs of *Atp1a3*, we
419 therefore could test the neuronal-specific role of the Na^+,K^+-ATPase in sleep.

420 Mutations in both zebrafish *Atp1a3* orthologs increased waking locomotor behaviour during
421 the day. However, only mutations in *atp1a3a,* which is expressed brain-wide, but not in
422 *atp1a3b*, which is expressed in more restricted brain regions, led to changes in night-time
423 sleep. The *atp1a3a* mutants have a larger sleep reduction than $dmist^{vir}$, $dmist^{i8}$, or $fxyd1^{\Delta 28}$
424 mutants, which is expected since loss of a pump subunit should have a larger effect than the
425 loss of a modulatory subunit, as has been shown for other ion channels (Cirelli et al., 2005;
426 Wu et al., 2014). Autosomal dominant missense mutations leading to loss of function in
427 *ATP1A3* cause movement disorders such as rapid-onset dystonia parkinsonism and childhood
428 alternating hemiplegia (recurrent paralysis on one side) in humans (Canfield et al., 2002;
429 Heinzen et al., 2014), while loss of function mutations in *Atp1a3* result in generalised seizures
430 and locomotor abnormalities, including hyperactivity, in mice, which was not observed in
431 zebrafish (Clapcote et al., 2009; Hunanyan et al., 2015; Ikeda et al., 2013; Kirshenbaum et al.,
432 2011; Sugimoto et al., 2014). A very high prevalence of insomnia was recently reported in
433 patients with childhood alternating hemiplegia, some of which harboured mutations in *Atp1a3*
434 (Kansagra et al., 2019), consistent with our observations that insomnia at night is a direct

435 behavioural consequence of *atp1a3a* mutation in zebrafish. Since zebrafish *atp1a3a* mutants
436 phenocopy the insomnia and hyperactivity phenotypes observed in patients, small molecule
437 screens aimed at ameliorating zebrafish *atp1a3a* mutant phenotypes may be a promising
438 approach for the rapid identification of new therapies for the management of this disease
439 (Hoffman et al., 2016; Rihel et al., 2010).

440 Together, the night-specific sleep phenotypes of *dmist*, *fxyd1*, and *atp1a3a* mutants point to
441 a role for the Na^+,K^+-ATPase in boosting sleep at night. How might the alpha3 catalytic subunit
442 of the Na^+/K^+ pump regulate sleep, and how could Dmist be involved? We found that Dmist is
443 required for proper maintenance of brain intracellular Na^+ levels at night but not during the day,
444 mirroring the timing of sleep disruption in *dmist*$^{i8/i8}$ animals. This suggests that the decreased
445 night-time sleep of *dmist* mutants is due to a specific requirement for Dmist modulation of the
446 Na^+/K^+ pump at night. However, we cannot exclude the possibility that Dmist's function is
447 required in only a subset of critical sleep/wake regulatory neurons during the day that then
448 influence behaviour at night, such as the wake-active, sleep-homeostatic regulating
449 serotonergic neurons of the raphe (Oikonomou et al., 2019) or wake-promoting Hcrt/orexin
450 neurons (Li et al., 2022). Another possibility is that disruption of proper establishment of the
451 Na^+ electrochemical gradient in *dmist* mutant neurons leads to dysfunction of various
452 neurotransmitter reuptake transporters, including those for glycine, GABA, glutamate,
453 serotonin, dopamine, and norepinephrine, which rely on energy from the Na^+ gradient to
454 function (Kristensen et al., 2011).

455 A third possibility is that Dmist and the Na^+,K^+-ATPase regulate sleep not by modulation of
456 neuronal activity per se but rather via modulation of extracellular ion concentrations. Recent
457 work has demonstrated that interstitial ions fluctuate across the sleep/wake cycle in mice. For
458 example, extracellular K^+ is high during wakefulness, and cerebrospinal fluid containing the ion
459 concentrations found during wakefulness directly applied to the brain can locally shift neuronal

460 activity into wake-like states (Ding et al., 2016). Given that the Na^+,K^+-ATPase actively
461 exchanges Na^+ ions for K^+ , the high intracellular Na^+ levels we observe in *atp1a3a* and *dmist*
462 mutants is likely accompanied by high extracellular K^+. Although we can only speculate at this
463 time, a model in which extracellular ions that accumulate during wakefulness and then directly
464 signal onto sleep-regulatory neurons could provide a direct link between Na^+,K^+ ATPase
465 activity, neuronal firing, and sleep homeostasis. Such a model could also explain why
466 disruption of Fxyd1 in non-neuronal cells also leads to a reduction in night-time sleep.

467 In addition to decreased night-time sleep, we also observed that *dmist* mutants have an
468 exaggerated sleep rebound response following the high, widespread neuronal activity induced
469 by the GABA-receptor antagonist, PTZ. Since both Atp1a3a and Dmist were essential for re-
470 establishing proper brain intracellular Na^+ levels following PTZ exposure (Figure 6A), we
471 speculate that the exaggerated sleep rebound is a consequence of increased neuronal
472 depolarization due to defective Na^+ pump activity. This is consistent with our previous
473 observations that the intensity of brain-wide neuronal activity impacts the magnitude of
474 subsequent sleep rebound via engagement of the Galanin sleep-homeostatic output arm
475 (Reichert et al., 2019). Why does loss of *dmist* lead to both decreased night-time sleep and
476 increased sleep rebound in response to exaggerated neuronal activity during the day? One
477 possibility is that Na^+/K^+ pump complexes made up of different alpha and beta subunits may
478 be differentially required for maintaining Na^+ homeostasis under physiological conditions and
479 have different affinities for (or regulation by) Dmist. For example, the Atp1a1 subunit is
480 considered the Na^+/K^+ pump workhorse in neurons, while Atp1a3, which has a lower affinity
481 for Na^+ ions, plays an essential role in repolarizing neurons when Na^+ rapidly increases during
482 high levels of neuronal activity, such as after a seizure (Azarias et al., 2013). If Dmist
483 preferentially interacts with Atp1a3a subunit, with which the non-additive effect of *dmist* and
484 *atp1a3a* mutation on sleep is consistent , day-time sleep-related phenotypes in *dmist* mutants

485 might be uncovered only during physiological challenge. Conversely, neurons may be more
486 dependent on Atp1a3a and Dmist for sodium homeostasis at night due to changes in Na^+/K^+
487 pump composition, Dmist interactions, or ion binding affinities. For example, activity of the
488 Na^+/K^+ pump can be modulated by the circadian clock (Damulewicz et al., 2013; Nakashima
489 et al., 2018), changes in substrate availability, including ATP (reviewed in Therien and Blostein,
490 2000), or hormones (Ewart and Klip, 1995). Teasing out how Dmist modulation of the Na+/K+
491 pump changes across the day-night cycle, and in which neurons Dmist's function may be
492 particularly important at night, will require future investigation.

493 In conclusion, through a genetic screening strategy in zebrafish, we have identified a novel
494 brain expressed gene that encodes a small transmembrane protein regulator of night-time
495 sleep and wake behaviours. Future work will be required to uncover the precise signalling
496 dynamics by which Dmist regulates the Na^+,K^+-ATPase and sleep.

497

498 **Acknowledgements**

499 The initial screen, discovery, and characterization of *dreammist* was conducted in the lab of
500 Alexander F Schier at Harvard University. We also would like to thank members of the Rihel
501 lab and other UCL zebrafish groups for helpful comments on experiments and the manuscript.
502 We thank Shannon Shibata-Germanos for *fxyd1* mutant tracking experiments, John
503 Parnavalas for reagents, Christine Orengo for help with small peptide sequence searches,
504 Stuart Peirson for early access to mouse transcriptomic data, and Finn Mango Bamber for the
505 Pokémon-card inspired *dreammist* name. The work was funded by NIH grants awarded to
506 Alexander Schier (GM085357 and HL10952505); an ERC Starting Grant (#282027) and
507 Wellcome Trust Investigator Award (#217150/Z/19/Z) to JR; NIH grant R35 NS122172 to DAP;
508 and a Grand Challenges PhD studentship to ILB.

509

510 **REFERENCES**

511 Aday, A.W., Zhu, L.J., Lakshmanan, A., Wang, J., and Lawson, N.D., 2011. Identification of
512 cis regulatory features in the embryonic zebrafish genome through large-scale profiling
513 of H3K4me1 and H3K4me3 binding sites. Dev. Biol. 357, 450–462.
514 https://doi.org/10.1016/j.ydbio.2011.03.007

515 Allebrandt, K. V, Amin, N., Müller-Myhsok, B., Esko, T., Teder-Laving, M., Azevedo,
516 R.V.D.M., Hayward, C., van Mill, J., Vogelzangs, N., Green, E.W., et al., 2013. A KATP
517 channel gene effect on sleep duration: from genome-wide association studies to function
518 in Drosophila. Mol. Psychiatry 18, 122–132. https://doi.org/10.1038/mp.2011.142

519 Azarias, G., Kruusmägi, M., Connor, S., Akkuratov, E.E., Liu, X.L., Lyons, D., Brismar, H.,
520 Broberger, C., and Aperia, A., 2013. A specific and essential role for Na,K-ATPase α3 in
521 neurons co-expressing α1 and α3. J. Biol. Chem. 288, 2734–2743.
522 https://doi.org/10.1074/jbc.M112.425785

523 Barlow, I.L., and Rihel, J., 2017. Zebrafish sleep: from geneZZZ to neuronZZZ. Curr. Opin.
524 Neurobiol. 44, 65–71. https://doi.org/10.1016/j.conb.2017.02.009

525 Bushey, D., Huber, R., Tononi, G., and Cirelli, C., 2007. Drosophila Hyperkinetic mutants
526 have reduced sleep and impaired memory. J. Neurosci. 27, 5384–93.
527 https://doi.org/10.1523/JNEUROSCI.0108-07.2007

528 Canfield, V.A., Loppin, B., Thisse, B., Thisse, C., Postlethwait, J.H., Mohideen, M.-A.P..,
529 Rajarao, S.J.R., and Levenson, R., 2002. Na,K-ATPase α and β subunit genes exhibit
530 unique expression patterns during zebrafish embryogenesis. Mech. Dev. 116, 51–59.
531 https://doi.org/10.1016/S0925-4773(02)00135-1

532 Chang, J.T., Lowery, L.A., and Sive, H., 2012. Multiple roles for the Na,K-ATPase subunits,
533 Atp1a1 and Fxyd1, during brain ventricle development. Dev. Biol. 368, 312–22.
534 https://doi.org/10.1016/j.ydbio.2012.05.034

535 Chemelli, R.M., Willie, J.T., Sinton, C.M., Elmquist, J.K., Scammell, T., Lee, C., Richardson,
536 J.A., Clay Williams, S., Xiong, Y., Kisanuki, Y., et al., 1999. Narcolepsy in orexin
537 knockout mice: Molecular genetics of sleep regulation. Cell 98, 437–451.
538 https://doi.org/10.1016/S0092-8674(00)81973-X

539 Chew, G.-L., Pauli, A., Rinn, J.L., Regev, A., Schier, A.F., and Valen, E., 2013. Ribosome
540 profiling reveals resemblance between long non-coding RNAs and 5' leaders of coding

541 RNAs. Development 140, 2828–34. https://doi.org/10.1242/dev.098343

542 Chiu, C.N., Rihel, J., Lee, D.A., Singh, C., Mosser, E.A., Chen, S., Sapin, V., Pham, U.,
543 Engle, J., Niles, B.J., et al., 2016. A Zebrafish Genetic Screen Identifies Neuromedin U
544 as a Regulator of Sleep/Wake States. Neuron 89, 842–856.
545 https://doi.org/10.1016/j.neuron.2016.01.007

546 Cirelli, C., 2009. The genetic and molecular regulation of sleep: from fruit flies to humans.
547 Nat. Rev. Neurosci. 10, 549–60. https://doi.org/10.1038/nrn2683

548 Cirelli, C., Bushey, D., Hill, S., Huber, R., Kreber, R., Ganetzky, B., and Tononi, G., 2005.
549 Reduced sleep in Drosophila Shaker mutants. Nature 434, 1087–1092.
550 https://doi.org/10.1038/nature03486

551 Clapcote, S.J., Duffy, S., Xie, G., Kirshenbaum, G., Bechard, A.R., Schack, V.R., Petersen,
552 J., Sinai, L., Saab, B.J., Lerch, J.P., et al., 2009. Mutation I810N in the α3 isoform of
553 Na+,K +-ATPase causes impairments in the sodium pump and hyperexcitability in the
554 CNS. Proc. Natl. Acad. Sci. U. S. A. 106, 14085–14090.
555 https://doi.org/10.1073/pnas.0904817106

556 Clausen, M. V, Hilbers, F., and Poulsen, H., 2017. The Structure and Function of the Na,K-
557 ATPase Isoforms in Health and Disease. Front. Physiol. 8, 371.
558 https://doi.org/10.3389/fphys.2017.00371

559 Crambert, G., Fuzesi, M., Garty, H., Karlish, S., and Geering, K., 2002. Phospholemman
560 (FXYD1) associates with Na,K-ATPase and regulates its transport properties. Proc. Natl.
561 Acad. Sci. U. S. A. 99, 11476–81. https://doi.org/10.1073/pnas.182267299

562 Damulewicz, M., Rosato, E., and Pyza, E. (2013). Circadian regulation of the Na+/K+-
563 ATPase alpha subunit in the visual system is mediated by the pacemaker and by retina
564 photoreceptors in Drosophila melanogaster. PLoS One 8, e73690.

565 Dashti, H.S., Jones, S.E., Wood, A.R., Lane, J.M., van Hees, V.T., Wang, H., Rhodes, J.A.,
566 Song, Y., Patel, K., Anderson, S.G., et al. (2019). Genome-wide association study
567 identifies genetic loci for self-reported habitual sleep duration supported by
568 accelerometer-derived estimates. Nat Commun 10, 1100.

569 De Carvalho Aguiar, P., Sweadner, K.J., Penniston, J.T., Zaremba, J., Liu, L., Caton, M.,
570 Linazasoro, G., Borg, M., Tijssen, M.A.J., Bressman, S.B., et al., 2004. Mutations in the
571 Na+/K+-ATPase α3 gene ATP1A3 are associated with rapid-onset dystonia

572 parkinsonism. Neuron 43, 169–175. https://doi.org/10.1016/j.neuron.2004.06.028

573 Despa, S., Tucker, A.L., and Bers, D.M., 2008. Phospholemman-mediated activation of Na/K-
574 ATPase limits [Na]i and inotropic state during β-adrenergic stimulation in mouse
575 ventricular myocytes. Circulation 117, 1849–1855.
576 https://doi.org/10.1161/CIRCULATIONAHA.107.754051

577 Ding, F., O'donnell, J., Xu, Q., Kang, N., Goldman, N., and Nedergaard, M., 2016. Changes
578 in the composition of brain interstitial ions control the sleep-wake cycle. Science (80-.).
579 352, 550–555. https://doi.org/10.1126/science.aad4821

580 Doğanli, C., Beck, H.C., Ribera, A.B., Oxvig, C., and Lykke-Hartmann, K., 2013. α3Na+/K+-
581 ATPase deficiency causes brain ventricle dilation and abrupt embryonic motility in
582 zebrafish. J. Biol. Chem. 288, 8862–8874. https://doi.org/10.1074/jbc.M112.421529

583 Dostanic, I., J. Schultz Jel, J. N. Lorenz, and J. B. Lingrel. 2004. 'The alpha 1 isoform of
584 Na,K-ATPase regulates cardiac contractility and functionally interacts and co-localizes
585 with the Na/Ca exchanger in heart', *J Biol Chem*, 279: 54053-61.Douglas, C.L.,
586 Vyazovskiy, V., Southard, T., Chiu, S.-Y., Messing, A., Tononi, G., and Cirelli, C., 2007.
587 Sleep in Kcna2 knockout mice. BMC Biol. 5, 42. https://doi.org/10.1186/1741-7007-5-42

588 Ewart, H.S., and Klip, A. (1995). Hormonal regulation of the Na(+)-K(+)-ATPase:
589 mechanisms underlying rapid and sustained changes in pump activity. Am J Physiol 269,
590 C295-311.

591 Feschenko, M.S., Donnet, C., Wetzel, R.K., Asinovski, N.K., Jones, L.R., and Sweadner,
592 K.J., 2003. Phospholemman, a single-span membrane protein, is an accessory protein
593 of Na,K-ATPase in cerebellum and choroid plexus. J. Neurosci. 23, 2161–2169.
594 https://doi.org/10.1523/jneurosci.23-06-02161.2003

595 Funato, H., Miyoshi, C., Fujiyama, T., Kanda, T., Sato, M., Wang, Z., Ma, J., Nakane, S.,
596 Tomita, J., Ikkyu, A., et al., 2016. Forward-genetics analysis of sleep in randomly
597 mutagenized mice. Nature 539, 378–383. https://doi.org/10.1038/nature20142

598 Gagnon, J.A., Valen, E., Thyme, S.B., Huang, P., Ahkmetova, L., Pauli, A., Montague, T.G.,
599 Zimmerman, S., Richter, C., and Schier, A.F., 2014. Efficient Mutagenesis by Cas9
600 Protein-Mediated Oligonucleotide Insertion and Large-Scale Assessment of Single-
601 Guide RNAs. PLoS One 9, e98186. https://doi.org/10.1371/journal.pone.0098186

602 Gandhi, A. V, Mosser, E.A., Oikonomou, G., and Prober, D.A., 2015. Melatonin Is Required

603 for the Circadian Regulation of Sleep. Neuron 85, 1–7.
604 https://doi.org/10.1016/j.neuron.2015.02.016

605 Geering, K., Béguin, P., Garty, H., Karlish, S., Füzesi, M., Horisberger, J.D., and Crambert,
606 G., 2003. FXYD proteins: New tissue- and isoform-specific regulators of Na,K-ATPase,
607 in: Annals of the New York Academy of Sciences. New York Academy of Sciences, pp.
608 388–394. https://doi.org/10.1111/j.1749-6632.2003.tb07219.x

609 Giraldez, A.J., Mishima, Y., Rihel, J., Grocock, R.J., Van Dongen, S., Inoue, K., Enright, A.J.,
610 and Schier, A.F., 2006. Zebrafish MiR-430 promotes deadenylation and clearance of
611 maternal mRNAs. Science 312, 75–79. https://doi.org/10.1126/science.1122689

612 Grunwald, H.A., Gantz, V.M., Poplawski, G., Xu, X.R.S., Bier, E., and Cooper, K.L., 2019.
613 Super-Mendelian inheritance mediated by CRISPR–Cas9 in the female mouse germline.
614 Nature. https://doi.org/10.1038/s41586-019-0875-2

615 Heinzen, E.L., Arzimanoglou, A., Brashear, A., Clapcote, S.J., Gurrieri, F., Goldstein, D.B.,
616 Jóhannesson, S.H., Mikati, M.A., Neville, B., Nicole, S., et al., 2014. Distinct neurological
617 disorders with ATP1A3 mutations. Lancet. Neurol. 13, 503–14.
618 https://doi.org/10.1016/S1474-4422(14)70011-0

619 Heinzen, E.L., Swoboda, K.J., Hitomi, Y., Gurrieri, F., De Vries, B., Tiziano, F.D., Fontaine,
620 B., Walley, N.M., Heavin, S., Panagiotakaki, E., et al., 2012. De novo mutations in
621 ATP1A3 cause alternating hemiplegia of childhood. Nat. Genet. 44, 1030–1034.
622 https://doi.org/10.1038/ng.2358

623 Hoffman, E.J., Turner, K.J., Fernandez, J.M., Cifuentes, D., Ghosh, M., Ijaz, S., Jain, R.A.,
624 Kubo, F., Bill, B.R., Baier, H., et al., 2016. Estrogens Suppress a Behavioral Phenotype
625 in Zebrafish Mutants of the Autism Risk Gene, CNTNAP2. Neuron 89, 725–733.
626 https://doi.org/10.1016/j.neuron.2015.12.039

627 Hunanyan, A.S., Fainberg, N.A., Linabarger, M., Arehart, E., Leonard, A.S., Adil, S.M.,
628 Helseth, A.R., Swearingen, A.K., Forbes, S.L., Rodriguiz, R.M., et al., 2015. Knock-in
629 mouse model of alternating hemiplegia of childhood: Behavioral and electrophysiologic
630 characterization. Epilepsia 56, 82–93. https://doi.org/10.1111/epi.12878

631 Iannacone, M.J., Beets, I., Lopes, L.E., Churgin, M.A., Fang-Yen, C., Nelson, M.D., Schoofs,
632 L., and Raizen, D.M., 2017. The RFamide receptor DMSR-1 regulates stress-induced
633 sleep in C. elegans. Elife 6. https://doi.org/10.7554/eLife.19837

634 Ikeda, K., Satake, S., Onaka, T., Sugimoto, H., Takeda, N., Imoto, K., and Kawakami, K.,
635 2013. Enhanced inhibitory neurotransmission in the cerebellar cortex of Atp1a3-deficient
636 heterozygous mice. J. Physiol. 591, 3433–3449.
637 https://doi.org/10.1113/jphysiol.2012.247817

638 Jansen, P.R., Watanabe, K., Stringer, S., Skene, N., Bryois, J., Hammerschlag, A.R., de
639 Leeuw, C.A., Benjamins, J.S., Muñoz-Manchado, A.B., Nagel, M., et al., 2019. Genome-
640 wide analysis of insomnia in 1,331,010 individuals identifies new risk loci and functional
641 pathways. Nat. Genet. 51, 394–403. https://doi.org/10.1038/s41588-018-0333-3

642 Jao, L.-E., Wente, S.R., and Chen, W., 2013. Efficient multiplex biallelic zebrafish genome
643 editing using a CRISPR nuclease system. Proc. Natl. Acad. Sci. U. S. A. 110, 13904–9.
644 https://doi.org/10.1073/pnas.1308335110

645 Johnson, L.S., Eddy, S.R., and Portugaly, E., 2010. Hidden Markov model speed heuristic
646 and iterative HMM search procedure. BMC Bioinformatics 11, 431.
647 https://doi.org/10.1186/1471-2105-11-431

648 Joiner, W.J., 2016. Unraveling the Evolutionary Determinants of Sleep. Curr. Biol. 26,
649 R1073–R1087. https://doi.org/10.1016/j.cub.2016.08.068\

650 Jones, S.E., van Hees, V.T., Mazzotti, D.R., Marques-Vidal, P., Sabia, S., van der Spek, A.,
651 Dashti, H.S., Engmann, J., Kocevska, D., Tyrrell, J., et al. (2019). Genetic studies of
652 accelerometer-based sleep measures yield new insights into human sleep behaviour.
653 Nat Commun 10, 1585.

654 Jumper, J., R. Evans, A. Pritzel, T. Green, M. Figurnov, O. Ronneberger, K.
655 Tunyasuvunakool, R. Bates, A. Zidek, A. Potapenko, A. Bridgland, C. Meyer, S. A. A.
656 Kohl, A. J. Ballard, A. Cowie, B. Romera-Paredes, S. Nikolov, R. Jain, J. Adler, T. Back,
657 S. Petersen, D. Reiman, E. Clancy, M. Zielinski, M. Steinegger, M. Pacholska, T.
658 Berghammer, S. Bodenstein, D. Silver, O. Vinyals, A. W. Senior, K. Kavukcuoglu, P.
659 Kohli, and D. Hassabis. 2021. 'Highly accurate protein structure prediction with
660 AlphaFold', *Nature*, 596: 583-89.

661 Kansagra, S., Ghusayni, R., Kherallah, B., Gunduz, T., McLean, M., Prange, L., Kravitz,
662 R.M., and Mikati, M.A., 2019. Polysomnography findings and sleep disorders in children
663 with alternating hemiplegia of childhood. J. Clin. Sleep Med. 15, 65–70.
664 https://doi.org/10.5664/jcsm.7572

665 Katoh, K., and Toh, H., 2010. Parallelization of the MAFFT multiple sequence alignment
666 program. Bioinformatics. https://doi.org/10.1093/bioinformatics/btq224

667 Kempf, A., Song, S.M., Talbot, C.B., and Miesenböck, G., 2019. A potassium channel β-
668 subunit couples mitochondrial electron transport to sleep. Nature 568, 230–234.
669 https://doi.org/10.1038/s41586-019-1034-5

670 Kimmel, C.B., Ballard, W.W., Kimmel, S.R., Ullmann, B., and Schilling, T.F., 1995. Stages of
671 embryonic development of the zebrafish. Dev. Dyn. 203, 253–310.
672 https://doi.org/10.1002/aja.1002030302

673 Kirshenbaum, G.S., Clapcote, S.J., Duffy, S., Burgess, C.R., Petersen, J., Jarowek, K.J.,
674 Yücel, Y.H., Cortez, M.A., Snead, O.C., Vilsen, B., et al., 2011. Mania-like behavior
675 induced by genetic dysfunction of the neuron-specific Na+,K+-ATPase α3 sodium pump.
676 Proc. Natl. Acad. Sci. U. S. A. 108, 18144–18149.
677 https://doi.org/10.1073/pnas.1108416108

678 Koh, K., Joiner, W.J., Wu, M.N., Yue, Z., Smith, C.J., and Sehgal, A., 2009. Identification of
679 SLEEPLESS, a novel sleep promoting factor. Science (80-.). 321, 372–376.
680 https://doi.org/10.1126/science.1155942.Identification

681 Kristensen, A.S., Andersen, J., Jorgensen, T.N., Sorensen, L., Eriksen, J., Loland, C.J.,
682 Stromgaard, K., and Gether, U., 2011. SLC6 neurotransmitter transporters: Structure,
683 function, and regulation. Pharmacol. Rev. 63, 585–640.
684 https://doi.org/10.1124/pr.108.000869

685 Kwan, K.M., Fujimoto, E., Grabher, C., Mangum, B.D., Hardy, M.E., Campbell, D.S., Parant,
686 J.M., Yost, H.J., Kanki, J.P., and Chien, C.-B., 2007. The Tol2kit: a multisite gateway-
687 based construction kit for Tol2 transposon transgenesis constructs. Dev. Dyn. 236,
688 3088–99. https://doi.org/10.1002/dvdy.21343

689 Lane, J.M., Jones, S.E., Dashti, H.S., Wood, A.R., Aragam, K.G., van Hees, V.T., Strand,
690 L.B., Winsvold, B.S., Wang, H., Bowden, J., et al. (2019). Biological and clinical insights
691 from genetics of insomnia symptoms. Nat Genet 51, 387-393.

692 Lee, D.A., Andreev, A., Truong, T. V., Chen, A., Hill, A.J., Oikonomou, G., Pham, U., Hong,
693 Y.K., Tran, S., Glass, L., et al., 2017. Genetic and neuronal regulation of sleep by
694 neuropeptide VF. Elife 6. https://doi.org/10.7554/eLife.25727

695 Lek, M., Karczewski, K.J., Minikel, E. V., Samocha, K.E., Banks, E., Fennell, T., O'Donnell-

696 Luria, A.H., Ware, J.S., Hill, A.J., Cummings, B.B., et al., 2016. Analysis of protein-
697 coding genetic variation in 60,706 humans. Nature 536, 285–291.
698 https://doi.org/10.1038/nature19057

699 Lenz, O., Xiong, J., Nelson, M.D., Raizen, D.M., and Williams, J.A., 2015. FMRFamide
700 signaling promotes stress-induced sleep in Drosophila. Brain. Behav. Immun. 47, 141–
701 148. https://doi.org/10.1016/j.bbi.2014.12.028

702 Li SB, Damonte VM, Chen C, Wang GX, Kebschull JM, Yamaguchi H, Bian WJ, Purmann C,
703 Pattni R, Urban AE, Mourrain P, Kauer JA, Scherrer G, de Lecea L. Hyperexcitable arousal
704 circuits drive sleep instability during aging. Science. 2022 Feb 25;375(6583):eabh3021.

705 Lin, L., Faraco, J., Li, R., Kadotani, H., Rogers, W., Lin, X., Qiu, X., de Jong, P.J., Nishino, S.,
706 Mignot, E., et al., 1999. The sleep disorder canine narcolepsy is caused by a mutation in
707 the hypocretin (orexin) receptor 2 gene. Cell 98, 365–76. https://doi.org/10.1016/S0092-
708 8674(00)81965-0

709 Love, M.I., Huber, W., and Anders, S., 2014. Moderated estimation of fold change and
710 dispersion for RNA-seq data with DESeq2. Genome Biol. 15, 550.
711 https://doi.org/10.1186/s13059-014-0550-8

712 McGrail, K.M., Phillips, J.M., and Sweadner, K.J., 1991. Immunofluorescent localization of
713 three Na,K-ATPase isozymes in the rat central nervous system: Both neurons and glia
714 can express more than one Na,K-ATPase. J. Neurosci. 11, 381–391.
715 https://doi.org/10.1523/jneurosci.11-02-00381.1991

716 Montague, T.G., Cruz, J.M., Gagnon, J.A., Church, G.M., and Valen, E., 2014. CHOPCHOP:
717 a CRISPR/Cas9 and TALEN web tool for genome editing. Nucleic Acids Res. gku410-.
718 https://doi.org/10.1093/nar/gku410

719 Nakashima, A., Kawamoto, T., Noshiro, M., Ueno, T., Doi, S., Honda, K., Maruhashi, T.,
720 Noma, K., Honma, S., Masaki, T., et al. (2018). Dec1 and CLOCK Regulate Na(+)/K(+)-
721 ATPase beta1 Subunit Expression and Blood Pressure. Hypertension 72, 746-754.

722 Oikonomou, G., Altermatt, M., Zhang, R. wei, Coughlin, G.M., Montz, C., Gradinaru, V., and
723 Prober, D.A., 2019. The Serotonergic Raphe Promote Sleep in Zebrafish and Mice.
724 Neuron 103, 686-701.e8. https://doi.org/10.1016/j.neuron.2019.05.038

725 Palagini, L., Domschke, K., Benedetti, F., Foster, R.G., Wulff, K., and Riemann, D., 2019.

726 Developmental pathways towards mood disorders in adult life: Is there a role for sleep
727 disturbances? J. Affect. Disord. 243, 121–132.
728 https://doi.org/10.1016/J.JAD.2018.09.011

729 Pauli, A., Valen, E., Lin, M.F., Garber, M., Vastenhouw, N.L., Levin, J.Z., Fan, L., Sandelin,
730 A., Rinn, J.L., Regev, A., et al., 2012. Systematic identification of long noncoding RNAs
731 expressed during zebrafish embryogenesis Systematic identification of long noncoding
732 RNAs expressed during zebrafish embryogenesis 577–591.
733 https://doi.org/10.1101/gr.133009.111

734 Pauli, A., Valen, E., and Schier, A.F., 2015. Identifying (non-)coding RNAs and small
735 peptides: Challenges and opportunities. BioEssays 37, 103–112.
736 https://doi.org/10.1002/bies.201400103

737 Pavlovic, D., Fuller, W., and Shattock, M.J., 2013. Novel regulation of cardiac Na pump via
738 phospholemman. J. Mol. Cell. Cardiol. 61, 83–93.
739 https://doi.org/10.1016/j.yjmcc.2013.05.002

740 Peyron, C., Faraco, J., Rogers, W., Ripley, B., Overeem, S., Charnay, Y., Nevsimalova, S.,
741 Aldrich, M., Reynolds, D., Albin, R., et al. (2000). A mutation in a case of early onset
742 narcolepsy and a generalized absence of hypocretin peptides in human narcoleptic
743 brains. Nat Med 6, 991-997.

744 Price, E. M., and J. B. Lingrel. 1988. 'Structure-function relationships in the Na,K-ATPase
745 alpha subunit: site-directed mutagenesis of glutamine-111 to arginine and asparagine-
746 122 to aspartic acid generates a ouabain-resistant enzyme', *Biochemistry*, 27: 8400-8.

747 Prober, D. a, Rihel, J., Onah, A. a, Sung, R.-J., and Schier, A.F., 2006. Hypocretin/orexin
748 overexpression induces an insomnia-like phenotype in zebrafish. J. Neurosci. 26,
749 13400–10. https://doi.org/10.1523/JNEUROSCI.4332-06.2006

750 Reichert, S., Pavón Arocas, O., and Rihel, J., 2019. The Neuropeptide Galanin Is Required
751 for Homeostatic Rebound Sleep following Increased Neuronal Activity. Neuron 104, 370-
752 384.e5. https://doi.org/10.1016/j.neuron.2019.08.010

753 Rihel, J., Prober, D. a, Arvanites, A., Lam, K., Zimmerman, S., Jang, S., Haggarty, S.J.,
754 Kokel, D., Rubin, L.L., Peterson, R.T., et al., 2010. Zebrafish behavioral profiling links
755 drugs to biological targets and rest/wake regulation. Science 327, 348–51.
756 https://doi.org/10.1126/science.1183090

757 Rihel, J., and Schier, A.F., 2013. Sites of action of sleep and wake drugs: insights from model
758 organisms. Curr. Opin. Neurobiol. 23, 831–40.
759 https://doi.org/10.1016/j.conb.2013.04.010

760 Salles, P.A., Mata, I.F., Brunger, T., Lal, D., and Fernandez, H.H. (2021). ATP1A3-Related
761 Disorders: An Ever-Expanding Clinical Spectrum. Front Neurol 12, 637890.

762 Sakurai, T., 2013. Orexin deficiency and narcolepsy. Curr. Opin. Neurobiol. 23, 760–766.
763 https://doi.org/10.1016/j.conb.2013.04.007

764 Sehgal, A., and Mignot, E., 2011. Genetics of sleep and sleep disorders. Cell 146, 194–207.
765 https://doi.org/10.1016/j.cell.2011.07.004

766 Shah, A.N., Davey, C.F., Whitebirch, A.C., Miller, A.C., and Moens, C.B., 2015. Rapid
767 reverse genetic screening using CRISPR in zebrafish. Nat. Methods 12, 535–540.
768 https://doi.org/10.1038/nmeth.3360

769 Shankaran, S.S., Dahlem, T.J., Bisgrove, B.W., Yost, H.J., and Tristani-Firouzi, M., 2017.
770 CRISPR/Cas9-Directed Gene Editing for the Generation of Loss-of-Function Mutants in
771 High-Throughput Zebrafish F_0 Screens, in: Current Protocols in Molecular Biology. John
772 Wiley & Sons, Inc., Hoboken, NJ, USA, pp. 31.9.1-31.9.22.
773 https://doi.org/10.1002/cpmb.42

774 Singh, C., Oikonomou, G., and Prober, D.A. (2015). Norepinephrine is required to promote
775 wakefulness and for hypocretin-induced arousal in zebrafish. Elife *4*, e07000.

776 Singh, C., Rihel, J., and Prober, D.A., 2017. Neuropeptide Y Regulates Sleep by Modulating
777 Noradrenergic Signaling. Curr. Biol. 27, 3796-3811.e5.
778 https://doi.org/10.1016/J.CUB.2017.11.018

779 Sivasubbu, S., Balciunas, D., Amsterdam, A., and Ekker, S.C., 2007. Insertional mutagenesis
780 strategies in zebrafish. Genome Biol. https://doi.org/10.1186/gb-2007-8-s1-s9

781 Sugimoto, H., Ikeda, K., and Kawakami, K., 2014. Heterozygous mice deficient in Atp1a3
782 exhibit motor deficits by chronic restraint stress. Behav. Brain Res. 272, 100–110.
783 https://doi.org/10.1016/j.bbr.2014.06.048

784 Sweadner, K.J., and Rael, E., 2000. The FXYD gene family of small ion transport regulators
785 or channels: cDNA sequence, protein signature sequence, and expression. Genomics
786 68, 41–56. https://doi.org/10.1006/geno.2000.6274Therien, A.G., and Blostein, R.
787 (2000). Mechanisms of sodium pump regulation. Am J Physiol Cell Physiol *279*, C541-

788 566.

789 Thisse, B., Pflumio, S., Fürthauer, M., Loppin, B., Heyer, V., Degrave, A., Woehl, R., Lux, A.,
790 Steffan, T., Charbonnier, X.Q. and Thisse, C. (2001) Expression of the zebrafish
791 genome during embryogenesis (NIH R01 RR15402). ZFIN Direct Data Submission. .
792 (http://zfin.org).

793 Thisse, C., and Thisse, B., 2008. High-resolution in situ hybridization to whole-mount
794 zebrafish embryos. Nat. Protoc. 3, 59–69. https://doi.org/10.1038/nprot.2007.514

795 Toda, H., Williams, J.A., Gulledge, M., and Sehgal, A., 2019. A sleep-inducing gene, nemuri,
796 links sleep and immune function in Drosophila. Science 363, 509–515.
797 https://doi.org/10.1126/science.aat1650

798 Ulitsky, I., Shkumatava, A., Jan, C.H., Sive, H., and Bartel, D.P., 2011. Conserved function of
799 lincRNAs in vertebrate embryonic development despite rapid sequence evolution. Cell
800 147, 1537–1550. https://doi.org/10.1016/j.cell.2011.11.055

801 Varshney, G.K., Lu, J., Gildea, D.E., Huang, H., Pei, W., Yang, Z., Huang, S.C., Schoenfeld,
802 D., Pho, N.H., Casero, D., et al., 2013. A large-scale zebrafish gene knockout resource
803 for the genome-wide study of gene function. Genome Res. 23, 727–35.
804 https://doi.org/10.1101/gr.151464.112

805 Villalba, A., Coll, O., and Gebauer, F., 2011. Cytoplasmic polyadenylation and translational
806 control. Curr. Opin. Genet. Dev. 21, 452–457. https://doi.org/10.1016/j.gde.2011.04.006

807 Wilkinson, R.N., Elworthy, S., Ingham, P.W., and van Eeden, F.J.M., 2013. A method for
808 high-throughput PCR-based genotyping of larval zebrafish tail biopsies. Biotechniques
809 55, 314–316. https://doi.org/10.2144/000114116

810 Wu, M., Robinson, J.E., and Joiner, W.J., 2014. SLEEPLESS Is a Bifunctional Regulator of
811 Excitability and Cholinergic Synaptic Transmission. Curr. Biol. 24, 621–629.
812 https://doi.org/10.1016/j.cub.2014.02.026

813 Wu, R.S., Lam, I.I., Clay, H., Duong, D.N., Deo, R.C., and Coughlin, S.R., 2018. A Rapid
814 Method for Directed Gene Knockout for Screening in G0 Zebrafish. Dev. Cell 46, 112-
815 125.e4. https://doi.org/10.1016/j.devcel.2018.06.003

816 Zhang, Y., Chen, K., Sloan, S.A., Bennett, M.L., Scholze, A.R., O'Keeffe, S., Phatnani, H.P.,
817 Guarnieri, P., Caneda, C., Ruderisch, N., et al., 2014. An RNA-sequencing transcriptome
818 and splicing database of glia, neurons, and vascular cells of the cerebral cortex. J.

819 Neurosci. 34, 11929–11947. https://doi.org/10.1523/JNEUROSCI.1860-14.2014

820

821 **Materials and Methods**

822 *Zebrafish husbandry*

823 All zebrafish lines were housed on a 14hr:10hr light:dark schedule in dechlorinated water at
824 27.5°C and routine husbandry was performed by the UCL Zebrafish Facility. Embryos were
825 collected from spontaneous spawning and staged according to Kimmel et al. 1995.

826 Embryos and larvae were raised on a 14hr:10hr light:dark schedule in 10cm Petri dishes at
827 a density of 50 embryos per 10cm Petri dish. Embryo water (~pH7.3, temperature 28.5°C,
828 conductivity ~423.7uS with methylene blue) was changed daily and animals over 4 days post
829 fertilisation were euthanized by overdose of MS-222 (300 mg/l) or 15% 2-Phenoyethanol
830 (77699 SIGMA-ALDRICH) at the end of experiments.

831 Raising of genetically altered zebrafish and all experimental procedures were performed
832 under project licence 70/7612 and PA8D4D0E5 awarded to JR under the UK Animals
833 (Scientific Procedures) Act 1986 guidelines.

834 *Lines*

Strain designation	**Gene identifier**	**Additional Information**
10543/dmist^{vir}	ENSDARG00000095754	Line maintained at Rihel lab
dmist^{i8}	ENSDARG00000095754	Line maintained at Rihel lab
fxyd1$^{\Delta 28}$	ENSDARG00000099014	Line maintained at Rihel lab
atp1a3a$^{\Delta 19}$	ENSDARG00000018259	Line maintained at Rihel lab
atp1a3b $^{\Delta 14}$	ENSDARG00000104139	Line maintained at Rihel lab

835 Table 1. Zebrafish lines

836 The *dmist*^{vir} allele was generated in wild type line T/AB-5 (Varshney et al., 2013) and
837 outcrossed to Harvard AB. The *dmist*^{i8}, *fxyd1* $^{\Delta 28}$, *atp1a3a*$^{\Delta 19}$, and *atp1a3b* $^{\Delta 14}$ alleles were
838 generated and maintained at UCL on an AB/TL background. Both *dmist*^{i8} and *dmist*^{vir} were out-
839 crossed to the AB strain at UCL for at least 3 generations.

840 *Larval Zebrafish Behavioural Tracking*

841 At 4 days post fertilisation (dpf), zebrafish larvae were placed into individual wells of a 96-
842 square well plate (WHA7701-1651 Sigma-Aldrich) filled with 650 µl of embryo water per well
843 and tracked for 3 days under a 14:10 light:dark schedule (lights on-09:00, lights off-23:00) using
844 automated videotracking in ViewPoint ZebraBoxes (Viewpoint Life Sciences). The 96-well plate
845 was under constant illumination with infrared LEDs, and white LEDs simulated the light:dark
846 schedule. Videography (with one-third inch Dragonfly2 PointGrey monochrome camera, frame
847 rate: 25-30 Hz; fixed-angle megapixel lens, Computar M5018-MP) of individual behavior was
848 recorded in quantization mode to detect movement by background subtraction between frames
849 in individual wells with 60 second integration time bins. Parameters used for detection were
850 calibrated according to the sensitivity of individual boxes but were in the following range:
851 detection threshold, 15-20; burst, 50 pixels; freeze, 3-4 pixels. Embryo water in the wells was
852 topped up daily with fresh water, and ambient room temperature was maintained at
853 approximately 26°C. Output data was sorted, parsed and analysed by custom Perl and Matlab
854 scripts (MATLAB R2016 version 9.1, The MathWorks), as in Rihel et al. 2010.

855 Oxygen-permeable lids (Applied Biosystems 4311971) were applied over the top of the 96-
856 well plate when performing experiments in constant darkness, and the larvae were left
857 undisturbed for the duration of the experiment to avoid light exposure.

858 At the end of the experiment, all larvae were visually checked for health before euthanasia
859 and transfer to individual wells of a 96-well PCR plate for DNA extraction and genotyping.

860 *Behavioural analysis*

861 Sleep parameters were calculated as in Rihel et al. 2010. For each genotype, exemplar
862 experiments are shown, and summary data was analysed by combining experiments with a
863 linear mixed effects model as follows. Behavioural summaries across multiple experiments
864 were determined by using the Matlab fitlme function to fit a linear mixed effects model for each
865 parameter with genotype as a fixed effect and independent experiment as a random effect,
866 then representing the effect size as a % change from the wild type value. Before fitting the
867 linear mixed effects model, the parameters sleep, sleep length, and waking activity were log
868 normalized by calculating the log of 1+ the parameter value for each larva.

869 Circadian period for every larva was calculated using the Matlab findpeaks function on the
870 activity (delta-pixels) timeseries data with a minimum peak distance of 18 hours (1080
871 minutes). N-way ANOVA was calculated to evaluate differences between groups.

872 Code and data are available at https://github.com/ilbarlow/Dmist.

873 *Adult behavioural tracking*

874 Fish from a *dmist*$^{i8/+}$ x *dmist*$^{i8/+}$ cross were raised in a mixed gender tank to adulthood.
875 Zebrafish adults (aged 3-4 months) were randomly selected and tracked on a 14:10 light:dark
876 cycle (180 lux at water surface, lit from above) for three days as in (Chiu et al., 2016). In brief,
877 fish were placed into uncovered plastic chambers (7x12x8.5 cm; WxLxH) with small holes for
878 water exchange, and these were placed in a circulating water tank (46x54 cm with 4.5 cm water
879 height). This setup was supplied with fish water from the home aquarium heated to 28ºC and
880 pumped from a 45 L reservoir at a flow rate of 1.3 L/min. Infrared light (60 degree, 54 LED
881 Video Camera Red Infrared Illuminator Lamp, SourcingMap, with the ambient light detector
882 covered) was continuously supplied from below. Fish were tracked at 15 Hz using Viewpoint
883 Life Sciences ZebraBox tracking software in tracking mode, with a background threshold of 40,
884 inactive cut-off of 1.3 cm/sec, and a small movement cut-off of 8 cm/sec. Each track was

885 visually inspected for errors at one-minute resolution across the entire session and analysed
886 using custom Matlab scripts (MATLAB R2016 version 9.1, The Mathworks, Inc). Experiments
887 were performed blind to genotype, which was determined by fin-clip after the experiment.
888 Females and males were originally analysed separately; since no significant gender effect was
889 found (two-way ANOVA, genotypeXgender), data from both genders were pooled for the final
890 analysis.

891 *Genotyping*

892 Prior to genotyping, adult fish were anaesthetised in 30 µg/ml MS-222, fin-clipped by cutting
893 a small section of the caudal fin, and then allowed to recover in fresh fish water. For pooled
894 experiments, 3 dpf larvae from heterozygous in-crosses were fin-clipped as in Wilkinson et al.,
895 2013 and allowed to recover in a square 96-well plate to keep larvae separate prior to pooling
896 larvae of the same genotype. Genomic DNA was extracted from adult fin clips and larvae by
897 boiling for 30 minutes in 50 µl 1X base solution (0.025 M KOH, 0.2 mM EDTA). Once cooled,
898 an equal volume (50 µl) of neutralisation buffer (0.04 M Tris-HCl) was then added and undiluted
899 genomic DNA used for genotyping.

900 The *dmist*^{vir} genotype was detected by PCR (standard conditions) using a cocktail of three
901 primers (0.36 mM final concentration each primer) to detect the wild type allele and viral
902 insertion (see Table 2) so that genotypes could be assigned according to size of bands
903 detected (*dmist*$^{vir/vir}$ 800 bp; *dmist*$^{vir/+}$ 508 bp and 800bp; *dmist*$^{+/+}$ 508 bp).

904 The *dmist*^{i8} genotype was assigned by KASP genotyping using allele-specific primers
905 (*dmist*^{i8} allele 5'-GATCTCCCT[GCAGAAAGAT]CTTTCTGCA-3' = FAM, *dmist*$^{+}$ allele 5'-
906 GATCTCCCT[CACCG]CTTTCTGCA-3' = HEX; KASP master mix KBS-1016-011) and assay
907 were prepared and analysed according to manufacturer's protocol (LGC genomics).

908 The *atp1a3a*$^{\Delta 19}$ genotype was assigned by KASP genotyping using allele-specific primers
909 (*atp1a3a*$^{\Delta 19}$ allele 5'-
910 GACAGACTGAAGAAACAGCGACTGACGGCTC[CAAAATGGGGGTAAGAGTC]-3' = FAM,
911 *atp1a3a*$^{+}$ allele 5'-GACAGACTGAAGAAACAGCGACTGACGGCTC-3'[] = HEX).

912 The *atp1a3b*$^{\Delta 14}$ genotype was assigned by PCR using MiSeq_atp1a3b primers (Table 2),
913 with the *atp1a3b*$^{\Delta 14}$ allele running 14 bp faster than the *atp1a3b*$^{+}$ allele.

914 *fxyd1*$^{\Delta 28}$ was assigned by KASP genotyping using allele-specific primers (*fxyd1*$^{\Delta 28}$ allele 5'-
915 GAAGGTCGGAGTCAACGGATTTAATAAACTTTATTGTGCTTTTGTAGTTGT[A]-3' = HEX,
916 *fxyd1*$^{+}$ allele 5'-
917 GAAGGTGACCAAGTTCATGCTTAATAAACTTTATTGTGCTTTTGTAGTTGT[G]-3' = FAM)
918 or PCR using MiSeq_fxyd1 primers (see Table 2) followed by digestion with the restriction
919 enzyme DrdI, which yields bands at 138 bp and 133 bp for *fxyd1*$^{+/+}$; 138 bp, 133 bp and 271
920 bp for *fxyd1*$^{+/\Delta 28}$, and 243 bp for *fxyd1*$^{\Delta 28}$.

921 *3'RACE*

922 FirstChoice RLM-RACE kit (Ambion AM1700) was used to amplify the 5' and 3' ends from
923 cDNA obtained from 4 dpf larvae raised on a 14:10 LD cycle and C57BL/6 E13.5 mouse
924 embryos obtained from the Parnavalas lab (UCL). 5' and 3' RACE primers were designed
925 according the manufacturer's guidelines (Table 2) and the manufacturer's protocol was
926 followed. Clones were sequenced by Sanger sequencing.

927 *In situ hybridisation*

928 Probes were designed to target the 3'UTR and entire open reading frame (ORF) of
929 *dmist_Dr* transcript using primers that amplified the target region from zebrafish cDNA under
930 standard PCR conditions (expected size 1325 bp; Table 2). The PCR product was cloned
931 into pSC vector (Strataclone PCR cloning kit Agilent 240205-12) and verified by Sanger

932 sequencing. Antisense probe was generated by cleavage of pSC-dmist plasmid with XbaI
933 and *in vitro* transcribed with T3 polymerase (Promega P2083) using 1 µg DNA template
934 according to the standard *in vitro* transcription protocol (see the full protocol at
935 dx.doi.org/10.17504/protocols.io.ba4pigvn). RNA probe was extracted and purified using the
936 ZYMO RNA concentrator kit (Zymo #R1013).

937 Whole mount *in situ* hybridisation was performed according to (Thisse and Thisse, 2008)
938 with the following adaptations. Embryos less than 5 dpf were dechorionated and fixed at the
939 appropriate stage in 4% paraformaldehyde (PFA) overnight at 4°C. 5 dpf larvae were fixed in
940 4% PFA/4% sucrose overnight at 4°C and then washed 3x5 min in PBS prior to dissecting out
941 the brain. Fixed embryos were washed 3x5 min in PBS, progressively dehydrated into 100%
942 methanol (MeOH) and stored at -20°C overnight. Prior to pre-hybridisation embryos were
943 bleached for 30 min in the dark (0.05% formamide, 0.5X SSC, 6% H_2O_2) and then fixed in 4%
944 PFA for 30 min at room temperature. To image, the embryos were progressively rehydrated
945 into 0.1% PBTw, progressively sunk in to 80% glycerol, and imaged on a Nikon compound
946 microscope (Nikon Eclipse Ni, Leica MC190HD camera).

947 *RT-qPCR*

948 Larvae from heterozygous in-crosses (*dmist*$^{i8/+}$ or *dmist*$^{vir/+}$) were genotyped by tail biopsy at
949 3 dpf (Wilkinson et al., 2013) and allowed to recover fully in individual wells of a square welled
950 96-well plate before euthanizing at 5 dpf. RNA was extracted from three 5 dpf embryos of each
951 genotype by snap freezing in liquid nitrogen and TRIzol RNA extraction (Ambion 15596026)
952 with the following modifications to the manufacturer's protocol: 400 µl total TRIzol reagent used
953 to homogenise larvae using a pellet pestle homogenizer, and 5 µg glycogen (Invitrogen Cat
954 No. 10814010; 20 µg/µl) was added to the RNA solution after chloroform extraction to aid
955 precipitation of the RNA. The cDNA library was synthesised from high quality RNA (Agilent
956 AffinityScript qPCR cDNA synthesis kit 600559), diluted 1:10, and gene-specific primers (Table

957 2) were used for amplification of target genes with SYBR green mastermix in a BioRad CFX
958 Real-Time qPCR instrument. Gene expression levels were normalised to the housekeeping
959 gene *ef1alpha* (primers in Table 2) and analysed using custom Matlab scripts (MATLAB v9.2
960 2017, The Mathworks 2017).

961 *Sodium Green Assay*

962 Cell permanent Sodium Green tetraacetate (Invitrogen, S6901) was prepared fresh from
963 frozen stock by dissolving in DMSO to 1 mM then diluting in fish water to a final concentration
964 of 10 µM. About 50 larvae (5-7 dpf) from *atp1a3a*$^{\Delta 19/+}$ or dmist$^{i8/+}$ in-crosses were placed in
965 wells of a 6 well plate, then most fish water was removed and replaced with 3 mL of the 10 µM
966 Sodium Green solution for two hours. During exposure, the plate was covered in foil and placed
967 in a 28°C incubator. For PTZ experiments, larvae were also exposed to 10 mM PTZ (diluted
968 from 1 mM stock dissolved in water) for two hours. For timepoints at night (ZT17-19), larvae
969 were handled and collected under red light. After soaking in Sodium Green, larvae were
970 washed 3X with fish water, anaesthetised with MS-2222, and fixed in 4% PFA/4% sucrose
971 overnight at 4°C. After 3X wash in PBS, larval brains were dissected and placed in 200 µL PBS
972 in a 48 well plate, and the matched bodies were used for genotyping (see *Genotyping*). Brains
973 were imaged using an upright MVX10 MacroView microscope with an MC PLAPO 1x objective
974 (both OLYMPUS) with a mercury lamp for fluorescent excitation at 488 nm (OLYMPUS, U-
975 HGLGPS). Images of roughly the same focal plane (dorsal/ventral view) were taken with an XM10
976 OLYMPUS camera by a single exposure following minimal light exposure (to avoid bleaching).
977 Mean fluorescent intensity was calculated from ROIs placed on the optic tectum/midbrain using
978 ImageJ, background subtracted and normalized to the average fluorescence intensity for each
979 imaging session.

980 *Protein Alignments*

981 Cross-species *dmist* homologues were identified by reciprocal BLASTp of the C-terminal
982 region of Dmist_*Dr* in vertebrate genomes. Translations of candidate transcript open reading
983 frames were then aligned with Dmist_*Dr* using ClustalOmega to calculate the percentage
984 identity matrix (www.ebi.ac.uk/Tools/msa/clustalo/) and visualised with the tool Multiple Align
985 Show (www.bioinformatics.org/sms/multi_align.html).

986 To identify Dmist orthologues, Dmist peptides were aligned with the multiple sequence
987 alignment tool MAFFT (Katoh and Toh, 2010) and seeded into a JackHMMR iterative search
988 of the Uniprot database (Johnson et al., 2010). Protein-protein alignments of Dmist to Fxyd1
989 were then performed using ClustalOmega and visualized with the tool Multiple Align Show.

990 *CRISPR/Cas9 gene targeting*

991 CRISPR targets were designed and synthesised according to Gagnon et al., 2014 using
992 ChopChop (Montague et al. 2014; http://chopchop.cbu.uib.no/; see Table 2 for sequences) to
993 identify target sites. 100 pg sgRNA and 300 pg Cas9 mRNA (pT3TS-nCas9n) were injected
994 into the yolk of 1-cell stage AB-TL embryos obtained from natural spawning. F0 fish were
995 screened by high resolution melt (HRM) analysis using gene-specific primers (Table 2) with
996 Precision melt supermix (Biorad 1725112) according to the manufacturer's protocol in a
997 BioRad CFX RT-PCR thermocycler. Positive founders identified in HRM analysis were then
998 sequenced by Illumina MiSeq using gene specific primers with adapters (Table 2) according to
999 the manufacturer's protocol.

1000 *Molecular cloning*

1001 GFP was fused to the Dmist_*Dr* open reading frame (ORF) by Gateway cloning (Kwan et
1002 al., 2007). Gene-specific primers were designed to amplify a PCR product that was recombined
1003 with middle donor vector (Table 2; Invitrogen Gateway pDONR221 Cat No. 12536017,
1004 Invitrogen Gateway BP Clonase II Cat No. 11789020) to generate a middle entry clone (pME-
1005 Dmist). pME-Dmist was recombined with 5' (p5E-CMV/SP6) and 3' (p3E-GFPpA) entry clones

1006 and destination vector (pDestTol2pA2) using Gateway Technology (Invitrogen LR Clonase II
1007 Plus enzyme Cat No. 12538200) following the manufacturer's protocol.

1008 A 3 bp mutation was introduced into the *CMV:dreammist-GFPpA* by inverse PCR using
1009 specific primers (Table 2) and KOD high fidelity hot start polymerase (Millipore 71085). The
1010 template was degraded by DpnI digest and circular PCR product was transformed into
1011 OneShot TOP10 chemically competent E coli (Invitrogen C4040). Both *CMV:dreammist-*
1012 *GFPpA* and *CMV:dreammistA22W-GFPpA* constructs were checked by Sanger sequencing.

1013 For labelling the plasma membrane, mRNA was *in vitro* transcribed from pCS2-myr-Cherry
1014 linearised with NotI, *in vitro* transcribed with SP6 mMessage mMachine (Ambion AM1340),
1015 purified and quantified with a QuBit spectrophotometer, and injected at 0.04 μg/μL.

1016 *Microinjection and imaging*

1017 For Dmist-GFP and DmistA22W-GFP live imaging, embryos from an AB-TL in-cross were
1018 injected with 1 nL of plasmid (7 ng/μL). After developing to 90% epiboly, the embryos were
1019 placed on a glass coverslip and observed on an inverted confocal microscope (SPinv, Leica)
1020 with a 40X objective.

1021 *RNAseq*

1022 Larvae from heterozygous in-crosses (*dmist*$^{i8/+}$ x *dmist*$^{i8/+}$ and *dmist*$^{vir/+}$ x *dmist*$^{vir/+}$) were
1023 raised to adulthood, genotyped and then homozygous mutant and wild type siblings were kept
1024 separate. Homozygous mutant and wild-type sibling fish were then in-crossed so that first
1025 cousins were directly compared. RNA was extracted from thirty 6 dpf larvae using the same
1026 protocol as for RT-qPCR and sent for RNAseq analysis at the UCL Institute of Child Health
1027 with a sequencing depth of 75 million reads per sample. Differential analysis of transcript count
1028 level between groups was performed as in (Love et al., 2014), and additional analysis was
1029 performed using custom Matlab scripts (MATLAB v9.2 2017, The Mathworks 2017).

1030 *Mouse RNAseq analysis*

1031 The dataset was downloaded from https://web.stanford.edu/group/barres_lab/
1032 brain_rnaseq.html; (Zhang et al., 2014) and hierarchical clustering (average linkage) and
1033 Pearson correlation calculation analysis were performed using custom Matlab scripts
1034 (MATLAB v9.2 2017, The Mathworks 2017).

1035 *Experimental Design and Statistical Analyses*

1036 Data was tested for normality using the Kolmogorov-Smirnov test. If data were normally
1037 distributed, N-way ANOVA (alpha=0.05) was used with correction for multiple comparisons
1038 using Tukey's test. If non-parametric, the Kruskal-Wallis test was used with correction for
1039 multiple comparisons using Dunn-Sidak (alpha=0.05). Outliers were removed by Grubb's test
1040 (threshold $p<0.01$). P values from the linear mixed effects models were determined by are an
1041 F-test on the fixed effects coefficients generated from the linear mixed effects model in Matlab.
1042 Data were grouped by genotype and gender for adult experiments and grouped by genotype
1043 and day of experiment for larval experiments.

1044 All code is available at https://github.com/ilbarlow/Dmist.

1045

1046 **Table 2. Primer Sequences**

1047

	Oligo Name	Sequence (5' -> 3')	Annealing temperature (oC)	Application
1	dmist_vir_fw	CACAGGGATGTGATGCCGGTTAAC	55	dmistvir genotyping
2	dmist_vir_rev	GTAGACACATACTGCCATACCAATC	55	dmistvir genotyping
3	vir_fw	CACCAGCTGAAGCCTATAGAGTACGAGC-	55	dmistvir genotyping
4	dmist_Dr_5RACE_fw	CGTTTCGCCACAATGTCAGCA	55-65	dmist_Dr 5'RACE
5	dmist_Dr_5RACE_rev_outer	AATGTTCAACTCCAGGCGTC	55-65	dmist_Dr 5'RACE
6	dmist_Dr_5RACE_rev_inner	AATGTTCAACTCCAGGCGTC	55-65	dmist_Dr 5'RACE
7	dmist_Dr_3RACE_fw_inner	GACGCCTGGAGTTGAACATT	55-65	dmist_Dr 3'RACE
8	dmist_Dr_3RACE_fw_outer	GGTATGGCAGTATGTGTCTACA	55-65	dmist_Dr 3'RACE
9	Dmist_Mm_3RACE_outer	GCTGGTGACTGTCCTCCTTATG	55-65	dmist_Mm 3'RACE
10	Dmist_Mm_3RACE_inner	GTGTCTACAAGCCCATCCGTC	55-65	dmist_Mm 3'RACE
11	dmist_Dr_fw	TTTCGCCACAATGTCAGCAGC	56	dmist_Dr probe
12	dmist_Dr_rev	CGACTTTCATTTATTAGTTCAGACATGTC	56	dmist_Dr probe
13	qPCR_dmist_fw	ACGCCAGACCTTATGAAATCC	60	RT-qPCR
14	qPCR_dmist_rev	TGCGTCGGAGAGGTTTGTAG	60	RT-qPCR
15	qPCR_ankrd13a_fw	TGGTGGCGTTCCAGAGTTAC	60	RT-qPCR
16	qPCR_ankrd13a_rev	GGACACGAGAGGAATCCAGC	60	RT-qPCR
17	qPCR_slc6a4b_fw	ACATGGTTGGGTCGACGTTT	60	RT-qPCR
18	qPCR_slc6a4b_rev	TCCAACCCACCAAAAGTGCT	60	RT-qPCR
19	ef1alpha_fw	TGCTGTGCGTGACATGAGGCAG	60	RT-qPCR
20	ef1alpha_rev	CCGCAACCTTTGGAACGGTGT	60	RT-qPCR
21	SP6dmist_sgRNA	ATTTAGGTGACACTATAGCGTTATGCAGAAAGCGGTGGTTTTAGAGCTAGAAATAGCAAG	n/a	CRISPR
22	T7atp1a3a_sgRNA	TAATACGACTCACTATAGACTGACGGCTCCAAAATGGGTTTTAGAGCTAGAAATAGCAAG	n/a	CRISPR
23	SP6fxyd1_sgRNA	ATTTAGGTGACACTATAGGACCCTCTGCCAACACAAGGTTTTAGAGCTAGAAATAGCAAG	n/a	CRISPR
24	SP6atp1a3b_sgRNA	ATTTAGGTGACACTATAGGACTGACTGCGCAACCATGGTTTTAGAGCTAGAAATAGCAAG	n/a	CRISPR
25	HRM_dmist_fw	GCCACAATGTCAGCAGCACG	59	HRM
26	HRM_dmist_rev	GCGTTCACTTTAGACTCTCCCAGC	59	HRM
27	HRM_atp1a3a_fw	TGACAGACTGAAGAAACAGC	55	HRM
28	HRM_atp1a3a_rev	TTAAATCTCAGCACCAGCAG5	55	HRM
29	HRM_fxyd1_fw	TGACCAAACCTTCTTAAGGTGC	58	HRM
30	HRM_fxyd1_rev	AAATTGAGAAGACTTACTGGTCTGC	58	HRM
31	HRM_atp1a3b_fw	AAAGGCTGTCACTTTCTCCATCAC5	58	HRM
32	HRM_atp1a3b_rev	TGCAGTAGATGAGGAATCGGTC	58	HRM
33	MiSeq_dmist_fw	TCGTCGGCAGCGTCAGATGTGTATAAGAGACAGTATAACTTACGTGTGGACGGACTC	58	MiSeq
34	MiSeq_dmist_rev	GTCTCGTGGGCTCGGAGATGTGTATAAGAGACAGTTGCCTCAGCAGGATTTCATAAG	58	MiSeq
35	MiSeq_atp1a3a_fw	TCGTCGGCAGCGTCAGATGTGTATAAGAGACAGTCGTTATCCGTGCAAGAGCTTC	58	MiSeq
36	MiSeq_atp1a3a_rev	GTCTCGTGGGCTCGGAGATGTGTATAAGAGACAGTTCTCAGCACCAGCAGTTATCG	58	MiSeq
37	MiSeq_atp1a3b_fw	TCGTCGGCAGCGTCAGATGTGTATAAGAGACAGTGACTGACATTCTCTCTTCGTG	68	MiSeq
38	MiSeq_atp1a3b_rev	GTCTCGTGGGCTCGGAGATGTGTATAAGAGACAGTTCTCTGTGATGCAGTAGATGAGG	68	MiSeq
39	MiSeq_fxyd1_fw	TCGTCGGCAGCGTCAGATGTGTATAAGAGACAGAAATACTGTCTTGTGACCAAACC	57	MiSeq
40	MiSeq_fxyd1_rev	GTCTCGTGGGCTCGGAGATGTGTATAAGAGACAGTTCATCCTCTGCTGCAAAATGC	57	MiSeq
41	attB1-dreammist forward primer	GGGGACAAGTTTGTACAAAAAAGCAGGCTTCACCATGTCAGCAGCACGCCTGATCTCC	55-60	Gateway
42	attB3-dreammist reverse primer	GGGGACCACTTTGTACAAGAAAGCTGGGTATCACCTGCGTCGGAGAGGTTTGTAG	55-60	Gateway
43	Dmist-GFPA22WFw	GCTTTTCCAGTCTGGGAGT**TGG**CAGCTGGGAGAGTCTAAAG	66	SDM
44	Dmist-GFPA22WRev	CTTTAGACTCTCCCAGCTG**CCA**ACTCCCAGACTGGAAAAGC	66	SDM

1048 **FIGURE LEGENDS**

1049

1050 **Figure 1. A viral insertion mini-screen identifies a short-sleeping mutant, *dreammist.***

1051 A-B) Mean± SEM sleep (A) and waking activity (B) of progeny from *dmist*$^{vir/+}$ in-cross from
1052 original screen. White blocks show day (lights on) and grey blocks show night (lights off). Data
1053 is combined from 2 independent experiments. n indicates the number of animals.

1054 C-F) Analysis of sleep/wake architecture for the data shown in (A, B). C) Quantification of total
1055 sleep across two days and nights shows decreased day and night sleep in *dmist*$^{vir/vir}$. Analysis
1056 of sleep architecture reveals fewer sleep bouts during the day (D) and shorter sleep bouts at
1057 night (E) in *dmist*$^{vir/vir}$ compared with sibling controls. F) Daytime waking activity is also
1058 increased in *dmist*$^{vir/vir}$. The black lines show the mean ± SEM, except in E, which labels the
1059 median ± SEM. *p<0.05, **p<0.01, ***p<0.001; ns p>0.05; one-way ANOVA, Tukey's post hoc
1060 test.

1061 G) Combining 5 independent experiments using a linear mixed effects model with genotype as
1062 a fixed effect and experiment as a random effect reveals *dmist*$^{vir/vir}$ larvae have decreased total
1063 sleep and changes to sleep architecture during both the day and night compared to *dmist*$^{+/+}$
1064 siblings. Plotted are the genotype effect sizes (95% confidence interval) for each parameter
1065 relative to wild type. Shading indicates day (white) and night (grey). P-values are assigned by
1066 an F-test on the fixed effects coefficients from the linear mixed effects model. *p<0.05,
1067 **p<0.01, ***p<0.001, ns p>0.05. n indicates the number of animals.

1068

1069

1070 **Figure 2. *dmist* encodes a conserved vertebrate single pass transmembrane protein.**

1071 A) *dmist* mutants harbour a viral insertion in the 1st intron of *si:key-234h16.7*. *dmist* is syntenic
1072 with *Ankrd13* and *GIT* orthologs in mouse, human, and zebrafish.

1073 B) RT-qPCR of *dmist* (red) show reduced expression of *dmist* and not the 5' and 3' flanking
1074 zebrafish genes, *slc6a4b* (cyan) and *ankrd13a* (blue), in $dmist^{vir/vir}$ larvae compared to $dmist^{vir/+}$
1075 and $dmist^{+/+}$ siblings. **p<0.01, *p<0.05; ns p>0.05; one-way ANOVA, Tukey's post-hoc test.
1076 Data shows mean ± SEM normalized to the wild type mean.

1077 C) *dmist_Dr* contains an open reading frame encoding a 70 amino acid protein that is
1078 conserved across vertebrates. All identified homologues have a predicted signal peptide
1079 sequence (magenta line), signal peptide cleavage site (magenta circle), and predicted
1080 transmembrane domain (grey), with additional highly conserved C-terminal motifs (blue lines).
1081 Identical amino acids in all species are shown in black; similar amino acids (80-99% conserved
1082 across species) are shown in grey.

1083 D) *In situ* hybridisation using a *dmist* antisense probe reveals *dmist* is maternally deposited as
1084 it is detected at the 2-cell stage. At 24 hpf expression is restricted to regions containing
1085 neuronal precursors, and at 5 dpf expression is widespread throughout the brain. Tel,
1086 telencephalon; Dien, diencephalon; R1-6, rhombomeres 1-6; A, anterior; P, posterior. Scale
1087 bars= 0.5 mm (2 cell and 24 hpf), 0.1 mm (5 dpf).

1088 E-F) Representative confocal image of 90% epiboly embryo co-injected at the 1-cell stage with
1089 mRNA encoding membrane-RFP (magenta) and a plasmid encoding either C-terminal tagged
1090 Dmist-GFP (E, green) or DmistA22W-GFP (F, green). Scale bar= 25 μm.

1091

1092 **Figure 3. CRISPR-generated *dmist* mutants sleep less and are hyperactive at night.**

1093 A) CRISPR/Cas9 targeting of the first exon of *dmist* resulted in an 8 bp insertion (*dmist*^{i8}) (grey
1094 line) within the coding sequence, leading to an early stop codon (red line with *). Guide RNA
1095 target sequence and PAM sequence are shown as black bars. The sequence that is deleted in
1096 the mutant is indicated with a red bar.

1097 B) Predicted Dmist^{i8} peptide sequence lacks most of the N-terminal signal peptide sequence
1098 (magenta) and the full C-terminus.

1099 C-D) Representative 48 hr traces of mean ± SEM sleep (C) and waking activity (D) shows
1100 decreased sleep and increased waking activity at night for *dmist*$^{i8/i8}$ fish compared to *dmist*$^{i8/+}$
1101 and *dmist*$^{+/+}$ siblings. n=number of fish.

1102 E-H) Analysis of sleep/wake architecture of the experiment depicted in (C, D) indicates that
1103 *dmist*$^{i8/i8}$ larvae sleep less at night (E) due to fewer sleep bouts (F). Sleep bout length is
1104 unchanged (G). Waking activity is also increased in *dmist*$^{i8/i8}$ fish (H). The black line represents
1105 the mean ± SEM except for G, which is the median ± SEM. *p<0.05, **p<0.01, ***p<0.001;
1106 One-way ANOVA, Tukey's post hoc test.

1107 I) Combining 5 independent experiments with a linear mixed effects model reveals *dmist*$^{i8/i8}$
1108 fish sleep less at night due to fewer sleep bouts and also show increased waking activity at
1109 night. Plotted are the genotype effect sizes (95% confidence interval) for each parameter
1110 relative to wild type. Shading indicates day (white) and night (grey). P-values are assigned by
1111 an F-test on the fixed effects coefficients from the linear mixed effects model. *p<0.05,
1112 **p<0.01, ***p<0.001, ns p>0.05.

1113 J-K) (J) Adult *dmist*$^{i8/i8}$ fish have a higher mean swim speed compared to their wild type siblings
1114 at night. Data in (J) is quantified at night in (K). (J, K) show mean ± SEM. *p<0.05, one-way
1115 ANOVA.

1116 L) Cumulative probability distribution of all night-time swim bout speeds in adult fish. The
1117 dashed lines show the half max (0.5 probability) for each curve. *p<0.05 for *dmist*$^{i8/i8}$ fish
1118 compared to wild type siblings; Kolmogorov-Smirnov test.

1119 **Figure 4. Mutation of the *dmist* related gene *fxyd1* causes reduced sleep at night.**

1120 A) Schematic of zebrafish Dmist and Fxyd1 protein domains and alignments comparing
1121 human, mouse, and zebrafish Dmist and FXYD1 protein sequences. Black and grey shading
1122 indicate amino acid identity and similarity, respectively. The FXYD domain is indicated with a
1123 red line and the RRR motif in the C-terminus is indicated with a dark blue line.

1124 B) CRISPR-Cas9 targeting of the 3rd exon of *fxyd1* created a 28 bp deletion, resulting in a
1125 predicted truncated protein. The start codon is marked by a cyan line. Guide RNA target
1126 sequence and PAM sequence are shown as black bars. The mutant deleted sequence is
1127 indicated with a red bar.

1128 C) *In situ* hybridisation of *fxyd1* at 24 hpf (whole animal) and 5 dpf brain (ventral view). Anterior
1129 is to the left. Scale bar = 0.5 mm (24 hpf); 0.1 mm (5 dpf).

1130 D-E) Representative behavioral experiment showing *fxyd1*$^{\Delta 28}$ mutants have decreased night-
1131 time sleep (D) but normal waking activity at night (E).

1132 F) Combining 5 independent experiments with a linear mixed effects model reveals *fxyd1*$^{\Delta 28/}$
1133 $^{\Delta 28}$ larvae sleep significantly less at night due to shorter sleep bouts compared to *fxyd1*$^{+/+}$
1134 siblings. Plotted are the genotype effect sizes (95% confidence interval) on each parameter
1135 relative to wild type. Shading indicates day (white) and night (grey). P-values are assigned by
1136 an F-test on the fixed effects coefficients from the linear mixed effects model. *p<0.05,
1137 **p<0.01, ***p<0.001, ns p>0.05.

1138

1139 **Figure 5. Mutation of the Na^+/K^+ pump alpha subunit *atp1a3a* reduces sleep at night**

1140 A-B) Mean ± SEM sleep and waking activity traces of wild type larvae following exposure to 1
1141 μM ouabain. Arrows indicate time the drug was added.

1142 C-D) At night, sleep is significantly reduced and waking activity is significantly increased after
1143 ouabain exposure. Student's t-test, one tailed.

1144 E) Alignments of Na^+/K^+ pump alpha subunits around the ouabain binding sites. Red indicates
1145 residues that are critical for higher sensitivity to ouabain, which are present in mouse Atp1a3
1146 but not Atp1a1.

1147 F) *In situ* hybridisation of *atp1a3a* at 24hpf (whole animal) and 5dpf brain (ventral view).
1148 Anterior is to the left. Scale bar = 0.5 mm (24 hpf); 0.1 mm (5 dpf). A-anterior; P-posterior; D-
1149 Dorsal; V-Ventral

1150 G) CRISPR-Cas9 targeting of the *atp1a3a* resulted in a 19 bp deletion that eliminates the start
1151 codon (blue) and splice junction. Guide RNA target sequence and PAM sequence are shown
1152 as black bars. Sequence that is deleted in the mutant is indicated with a red bar.

1153 H-I) Representative behavioural experiment showing *atp1a3a*$^{\Delta 19/\Delta 19}$ fish are hyperactive
1154 throughout the day-night cycle and have decreased sleep at night. Mean ± SEM are shown.

1155 J) *atp1a3a*$^{\Delta 19/\Delta 19}$ larvae sleep less at night due to shorter sleep bouts. Plotted are the genotype
1156 effect sizes (95% confidence interval) on each parameter relative to wild type. Shading
1157 indicates day (white) and night (grey). P-values are assigned by an F-test on the fixed effects
1158 coefficients from the linear mixed effects model. *$p<0.05$, **$p<0.01$, ***$p<0.001$, ns $p>0.05$.

1159

1160 **Figure 6. *dmist* mutants have altered sodium homeostasis**

1161 A) Brain sodium levels are significantly elevated after exposure to PTZ in both *atp1a3a*$^{\Delta 19/\Delta 19}$
1162 (2 independent experiments) and *dmist*$^{i8/i8}$ (4 independent experiments) fish relative to wild
1163 type and heterozygous mutant siblings, as measured by fluorescence intensity of Sodium
1164 Green, normalized to the sample mean intensity. Crosses show mean ± SEM. n indicated the
1165 number of animals. Below are example images of brains stained with Sodium Green. *p<0.05,
1166 **p<0.01, one-way ANOVA, Tukey's post hoc test.

1167 B) Under baseline conditions, brain sodium levels are significantly elevated in *dmist*$^{i8/i8}$ fish at
1168 night but not during the day, as measured by fluorescence intensity with Sodium Green.
1169 Crosses show mean ± SEM. *p<0.05, **p<0.01, one-way ANOVA, Tukey's post hoc test.

1170 C) *dmist*$^{i8/i8}$ larvae have increased rebound sleep compared to wild type siblings following
1171 exposure to 5mM PTZ. Representative sleep traces of *dmist*$^{+/+}$ (no drug, water vehicle controls
1172 in black; PTZ exposed in blue) and *dmist*$^{i8/i8}$ (no drug in purple; PTZ exposed in red) following
1173 1 hr exposure to 5 mM PTZ (black bar) in the morning. Data are mean ± SEM. *dmist*$^{i8/+}$ animals
1174 are not plotted for clarity but are included in panel D.

1175 D) Rebound sleep after exposure to 5 mM PTZ, calculated from the experiment in C. Each dot
1176 represents a single fish, grey lines show mean ± SEM.

1177 E) Effect size of change in sleep after 1 hr treatment with 5 mM PTZ (and washout) compared
1178 to vehicle treated controls (error bars show 95% confidence intervals). *p<0.05, one-way
1179 ANOVA, Tukey's post-hoc test.

1180 F) Effect sizes (and 95% confidence interval) relative to wild types (dotted line) on sleep at
1181 night in larvae from *dmist*$^{+/-}$; *atp1a3a*$^{+/-}$ in-crosses from 3 independent experiments. P-values
1182 are assigned by an F-test on the fixed effects coefficients from the linear mixed effects model
1183 relative to *dmist*$^{+/+}$; *atp1a3a*$^{+/+}$ animals. For all sleep-wake parameters, see Figure S6. *p<0.05,
1184 **p<0.01, ***p<0.0001, ns p>0.05.

1185 **Figure S1. A viral insertion screen for sleep-wake regulators**

1186 A) Schematic of screening strategy. Candidate genes were selected from a list of 904
1187 mammalian genes encoding protein classes most often linked to behavioural regulation,
1188 including 1) genes previously implicated in sleep and circadian rhythms; 2) G-protein coupled
1189 receptors; 3) neuropeptide ligands; 4) channels; and 5) proteins involved in post-translational
1190 regulation, such as de-ubiquitinating enzymes (Supplemental Data 1). tBLASTN of the human
1191 protein sequences identified 1162 zebrafish orthologs (Zv6), of which 702 (60.4%) had viral
1192 insertions mapped in the 'Zenemark' zebrafish viral insertion library (Varshney et al., 2013).
1193 Sperm harbouring viral insertions in 25 loci were successfully used for *in vitro* fertilization and
1194 propagated to the F3 generation for screening. F3 larvae from single family F2 in-crosses were
1195 monitored on a 14hr:10hr light:dark cycle from 4-7 dpf using videography and genotyped at the
1196 end of the experiment.

1197 B-C) Histogram of total daytime sleep (B) and average daytime waking activity (C) normalized
1198 as standard deviations from the mean (Z-score) of all the viral-insertion lines tested (including
1199 heterozygous *vir/+* and homozygous *vir/vir*). Line 10543 (renamed *dreammist*) exhibited
1200 decreased daytime sleep and increased daytime waking activity.

1201

1202 **Figure S2. *dmist*$^{vir/vir}$ fish are hyperactive and have normal circadian rhythms.**

1203 A) Free-running circadian period length of the locomotor activity of larvae from a *dmist*$^{vir/+}$ in-
1204 cross following the transition at 5 dpf from a 14hr:10hr light:dark cycle to constant dark
1205 conditions. The data is quantified for 48 hours after the shift to darkness and shows no
1206 difference in period between *dmist*$^{vir/vir}$ larvae and their sibling controls. Data is from 3
1207 independent experiments. $p>0.05$, one-way ANOVA, Tukey's post hoc test.

1208 B-C) Representative mean ± SEM sleep (B) and waking activity (C) traces of animals used to
1209 calculate circadian period length in (A). Light and dark grey blocks show subjective day and
1210 night, respectively.

1211 D) RT-qPCR time-course before (light) and after (grey) transfer into constant dark
1212 demonstrates that *dmist* mRNA levels do not oscillate with a circadian period, unlike *per1*
1213 mRNA which does. n=3 replicates per timepoint. Expression is normalized to circadian time 3.
1214 Data are mean ± SEM.

1215

1216 **Figure S3. *dmist* is enriched in neurons and requires the signal peptide cleavage site for**
1217 **membrane localisation**.
1218 A) Relative expression level of *dmist* transcript from RNA sequencing of 6 dpf *dmist*$^{vir/vir}$ and
1219 *dmist*$^{+/+}$ siblings. Z-scores were calculated by subtracting mean expression and normalising by
1220 the standard deviation across all expressed transcripts (27,243 transcripts). Data show mean
1221 ± SEM from 3 independent biological replicates. **p<0.01 Student's t-test.
1222 B) 3' and 5' RACE identify a long (1100 bp) and short (215 bp) 3'UTR variant in *dmist_Dr*, and
1223 a long 3'UTR (1050 bp) in *Dmist_Mm*. The purple arrow indicates the ISH probe used in Figure
1224 2D.
1225 C) *dmist_Dr* sense probe negative control at 24 hpf shows no detectable expression.
1226 D) Percentage identity matrix comparing *Dmist* homologues across 6 vertebrate species
1227 (100%=magenta; >70%=purple; >50%=cyan; <50%=green).
1228 E) Hierarchical clustering of RNAseq dataset of 6 different cell types isolated from the
1229 developing (E13.5) mouse brain (Zhang et al., 2014) and post-hoc identification of *Dmist_Mm*.
1230 Data was standardized by subtracting the mean expression and normalizing by the standard
1231 deviation across all expressed transcripts in each cell type (column). *Dmist_Mm* (green arrow)
1232 co-clusters with genes highly expressed in neurons (green shaded branches).
1233 F) Pearson rank correlation of canonical cell-type markers with *Dmist_Mm* shows high co-
1234 expression with neuronal markers compared to astroglial and endothelial cell markers. Data
1235 are mean ± SEM. *p<0.05, **p<0.01; Kruskal-Wallis, Dunn-Sidak post-hoc test.
1236 G-I) Predicted processing of Dmist to its mature form in the plasma membrane (G). C-terminal
1237 GFP fusion to Dmist is predicted to localise to the membrane (H). However, a mutation (A22W)
1238 at the signal peptide cleavage site (I) is predicted to inhibit signal peptide cleavage and so
1239 prevent proper subcellular localisation of the mature protein.

1240 **Figure S4. CRISPR-generated *dmist* mutants have reduced *dmist* transcript levels**

1241 A) RT-qPCR shows *dmist*$^{i8/i8}$ larvae have reduced *dmist* mRNA levels, suggesting that *dmist*^{i8}

1242 transcripts undergo nonsense mediated decay. Data are mean ± SEM of three biological

1243 replicates. **p<0.01; one-way ANOVA, Tukey's post-hoc test.

1244 B) Relative expression level of *dmist* transcript from RNA sequencing of 6 dpf *dmist*$^{i8/i8}$ and

1245 *dmist*$^{+/+}$ siblings. Z-score calculated by subtracting mean expression and normalising by the

1246 standard deviation across all expressed transcripts. Data are mean ± SEM for 3 independent

1247 biological replicates. **p<0.01, Student's t-test.

1248

1249

1250 **Figure S5. Ouabain dose curve and effects of *atp1a3b* mutation on behaviour.**

1251 A) Dose response curve of ouabain's effects on sleep at night, shown as mean ± SEM and
1252 normalized to the DMSO control. Each data point represents a single fish.

1253 B) Pearson rank correlation of canonical cell-type markers with *Atp1a3a_Mm* shows high co-
1254 expression with neuronal markers compared to astroglial and endothelial cell markers. Data
1255 are mean ± SEM.

1256 C) *In situ* hybridisation of *atp1a3a* at 24 hpf (whole animal) and 5 dpf brain (ventral view).
1257 Anterior is to the left. Scale bar = 0.5 mm (24 hpf); 0.1 mm (5 dpf).

1258 D) CRISPR-Cas9 targeting of *atp1a3b* resulted in a 14 bp deletion that eliminates the start
1259 codon (blue). Guide RNA target sequence and PAM sequence are shown as black bars. The
1260 sequence that is deleted in the mutant is indicated with a red bar.

1261 E-F) Representative single behavioural experiment showing *atp1a3b*$^{\Delta 14/\Delta 14}$ mutants have
1262 increased daytime waking activity but normal sleep patterns.

1263 G) Data from 2 independent experiments combined with a linear mixed effects model. Plotted
1264 are the genotype effect sizes (95% confidence interval) for each parameter relative to wild type
1265 (dotted line) for each genotype. Shading indicates day (white) and night (grey). n indicates the
1266 number of animals. P-values are assigned by an F-test on the fixed effects coefficients from
1267 the linear mixed effects model relative to *atp1a3b*$^{+/+}$ animals. *$p<0.05$.

1268

1269

1270 **Figure S6. Sleep effects in *dmist*$^{-/-}$; *atp1a3a*$^{-/-}$ double mutants are non-additive.**

1271 Combining 3 independent experiments with a linear mixed effects model reveals that the effects
1272 of loss of function *dmist* and *atp1a3a* mutations are non-additive. Plotted are the genotype
1273 effect sizes (95% confidence interval) for each parameter relative to wild type for each
1274 genotype. Shading indicates day (white) and night (grey). n indicates the number of animals.

1275

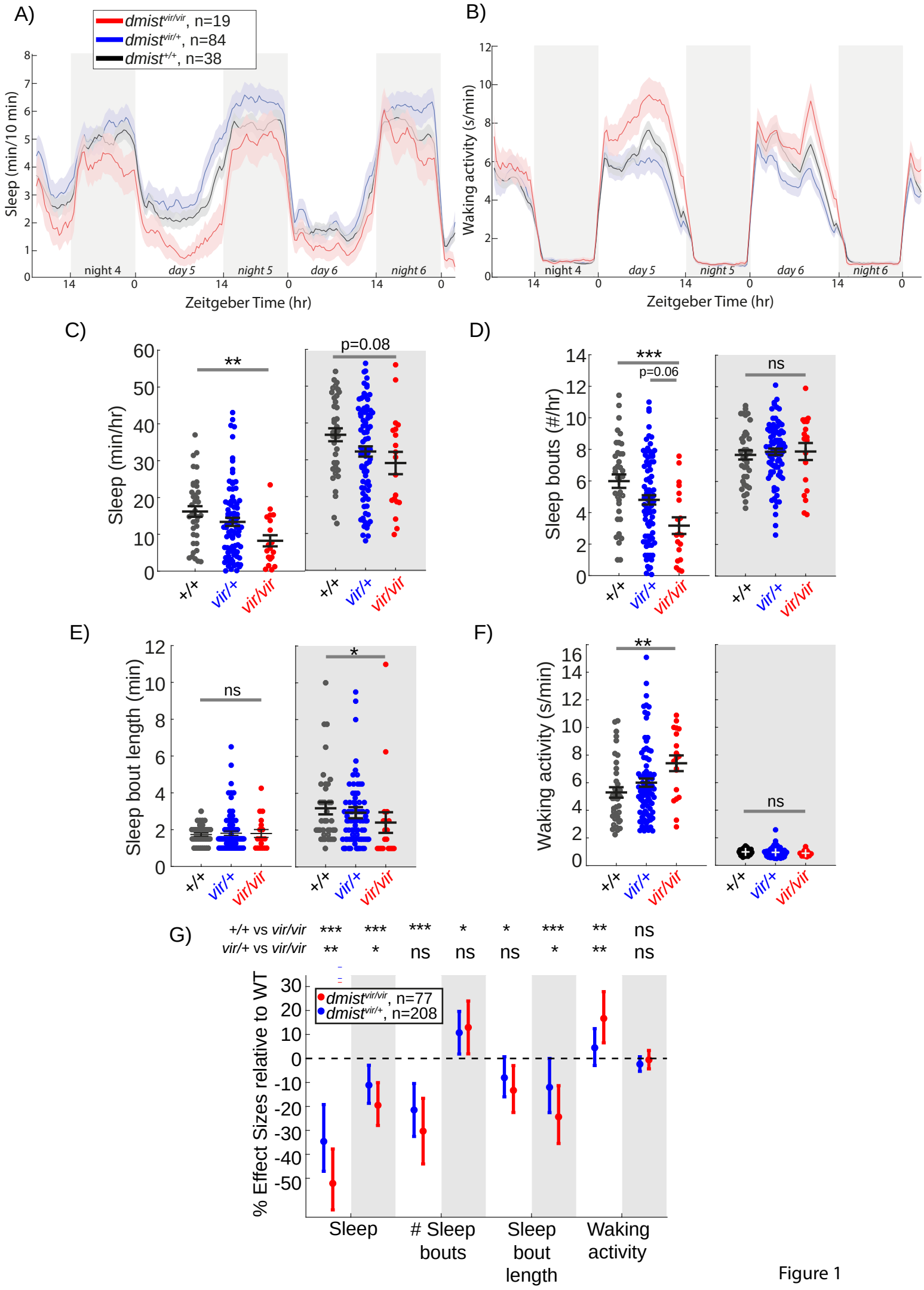
A)
dmist vir/vir, n=19
dmist vir/+, n=84
dmist +/+, n=38
Sleep (min/10 min)
night 4
day 5
night 5
day 6
night 6
Zeitgeber Time (hr)
B)
Waking activity (s/min)
C)
Sleep (min/hr)
**
p=0.08
D)
Sleep bouts (#/hr)
***
p=0.06
ns
E)
Sleep bout length (min)
ns
*
F)
Waking activity (s/min)
**
ns
+/+
vir/+
vir/vir
G)
+/+ vs vir/vir *** *** *** * * *** ** ns
vir/+ vs vir/vir ** * ns ns ns * ** ns
% Effect Sizes relative to WT
dmist vir/vir, n=77
dmist vir/+, n=208
Sleep
Sleep bouts
Sleep bout length
Waking activity

Figure 1

A)

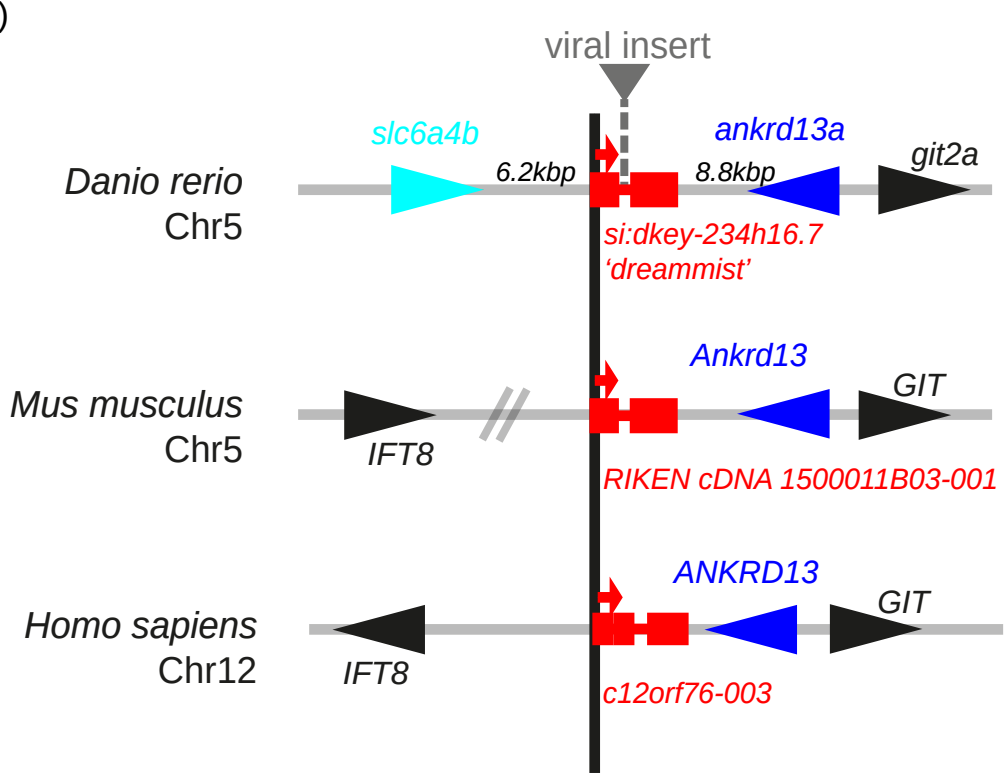

B)

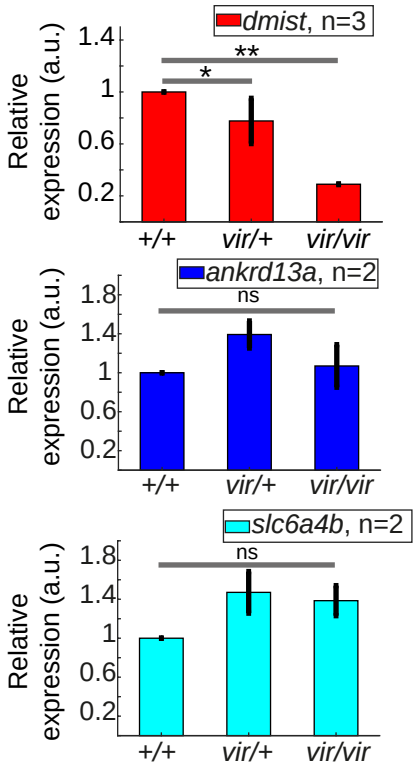

C)

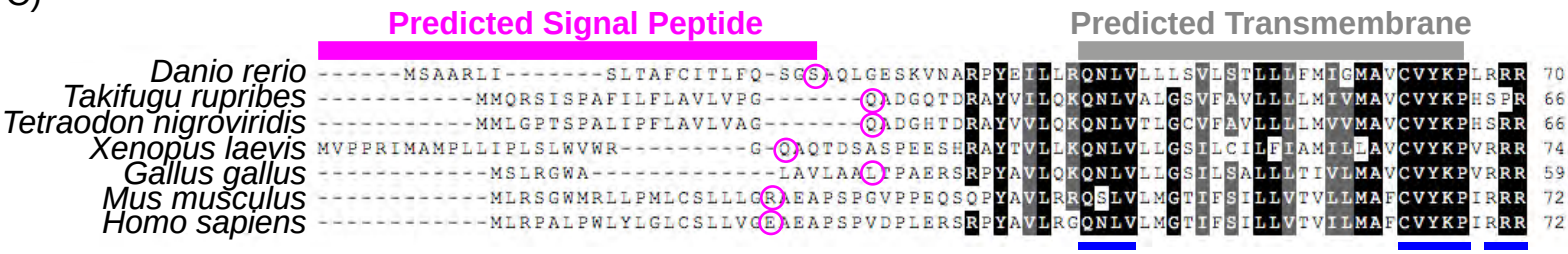

D)

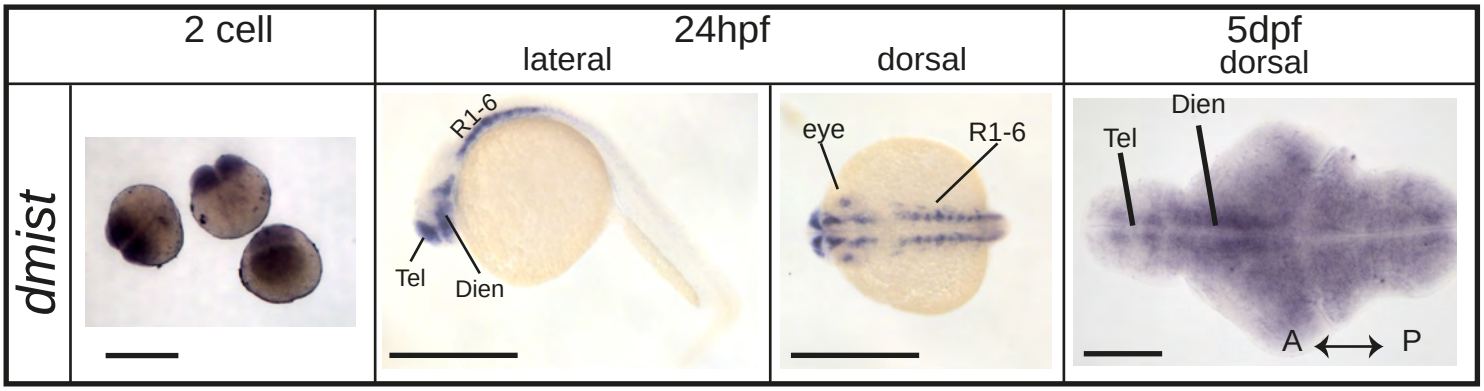

E)

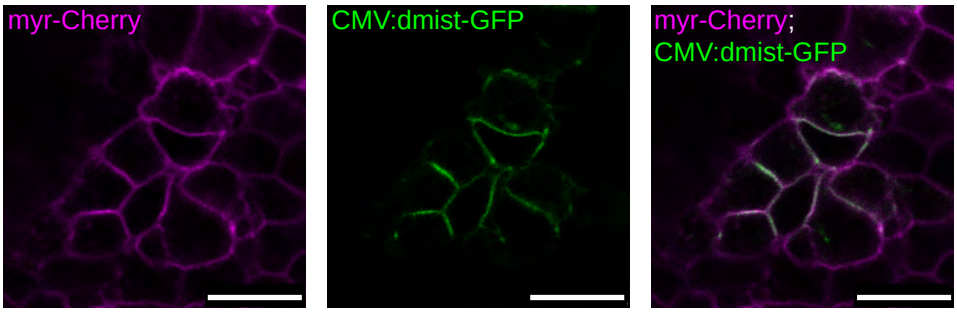

F)

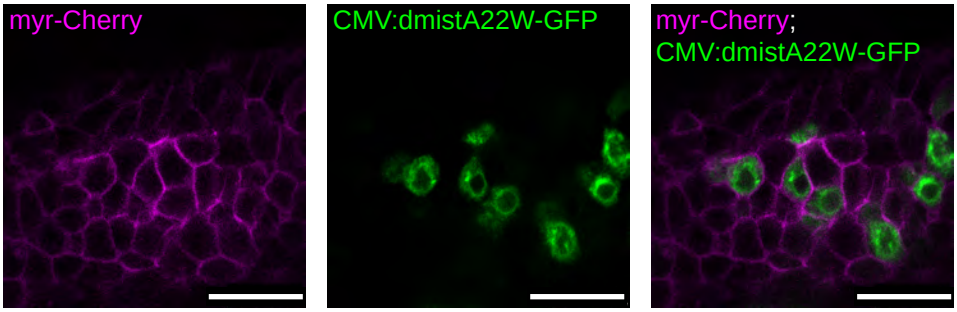

Figure 2

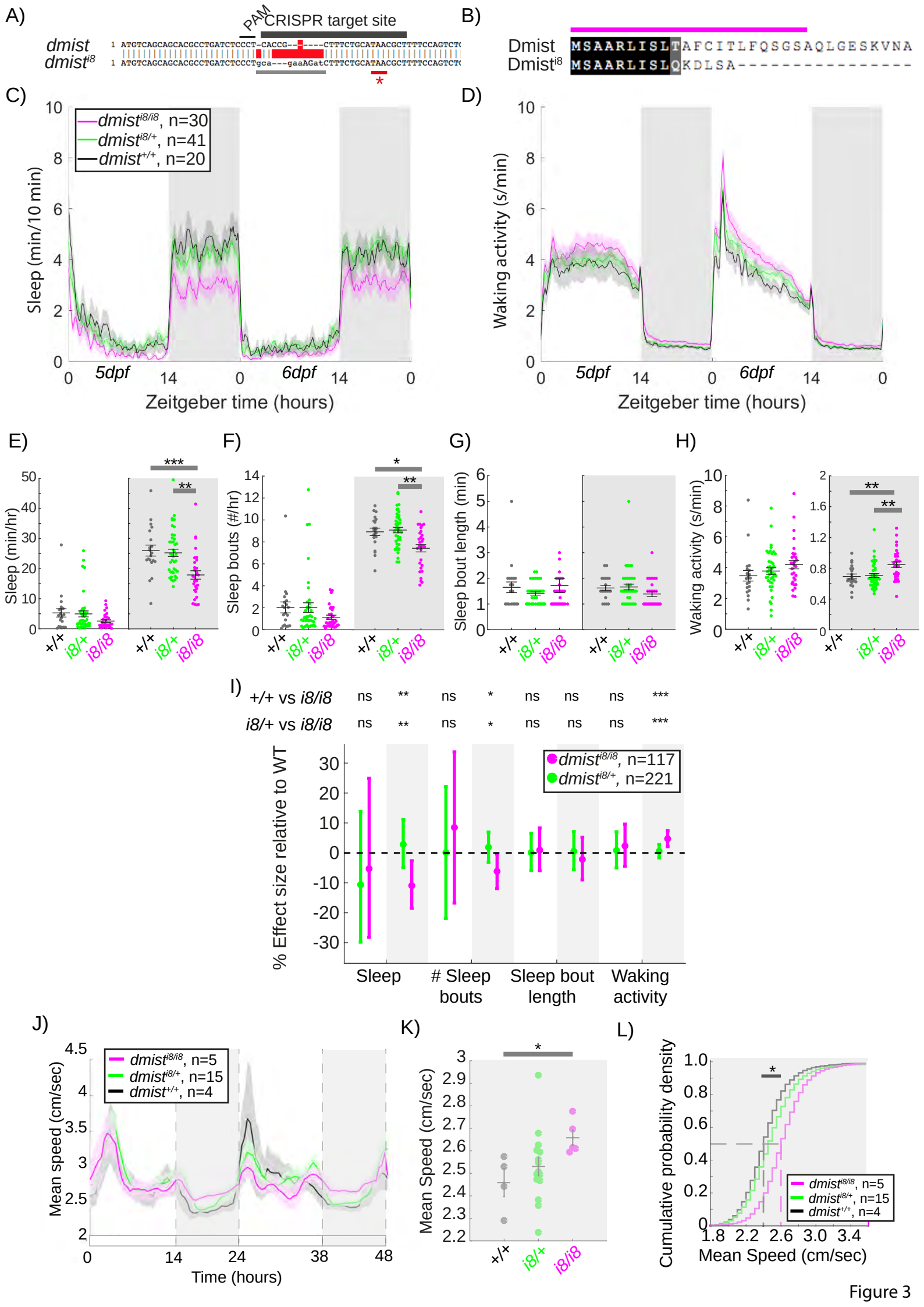
A)
PAM
CRISPR target site
dmist
dmist^i8
B)
Dmist
Dmist^i8
MSAARLISLTAFCITLFQSGSAQLGESKVNA
MSAARLISLQKDLSA
C)
dmist^i8/i8, n=30
dmist^i8/+, n=41
dmist^+/+, n=20
Sleep (min/10 min)
5dpf
6dpf
Zeitgeber time (hours)
D)
Waking activity (s/min)
Zeitgeber time (hours)
E)
Sleep (min/hr)
F)
Sleep bouts (#/hr)
G)
Sleep bout length (min)
H)
Waking activity (s/min)
+/+
i8/+
i8/i8
I)
+/+ vs i8/i8
i8/+ vs i8/i8
dmist^i8/i8, n=117
dmist^i8/+, n=221
% Effect size relative to WT
Sleep
Sleep bouts
Sleep bout length
Waking activity
J)
dmist^i8/i8, n=5
dmist^i8/+, n=15
dmist^+/+, n=4
Mean speed (cm/sec)
Time (hours)
K)
Mean Speed (cm/sec)
L)
Cumulative probability density
Mean Speed (cm/sec)

Figure 3

A)

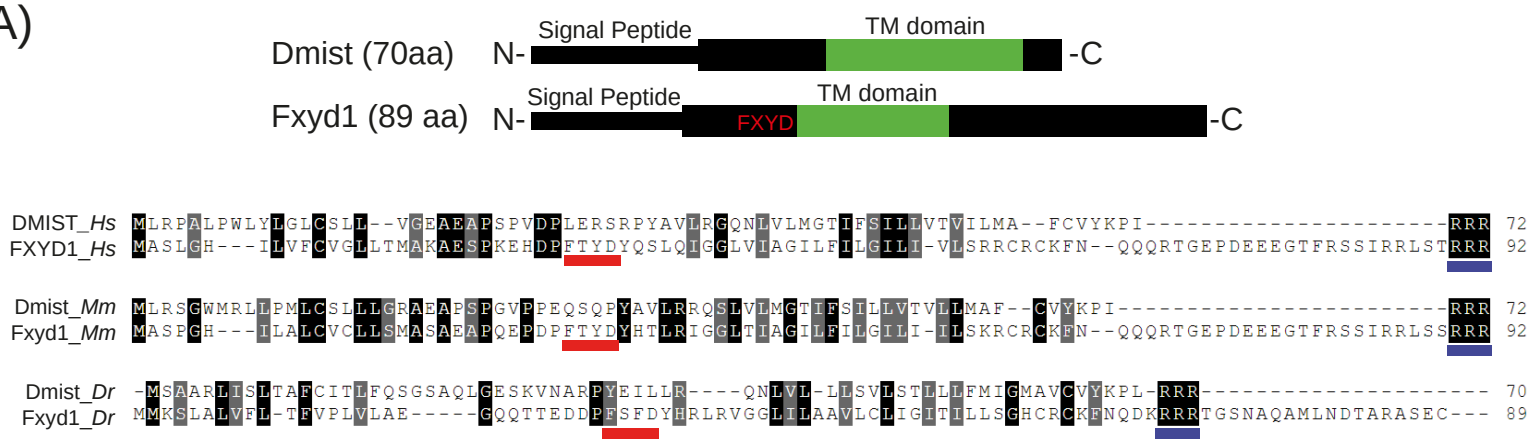

B)

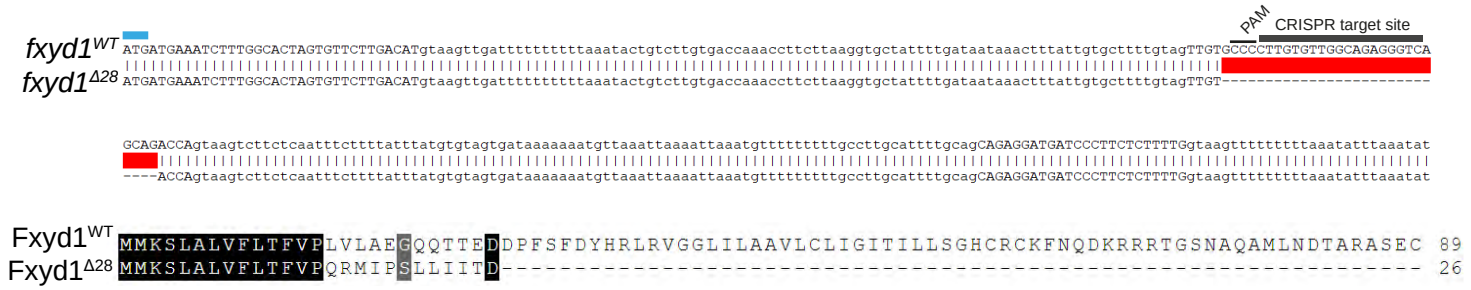

C)

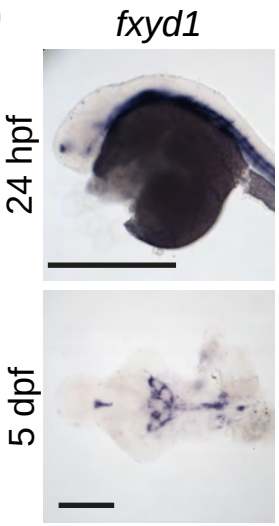

D)

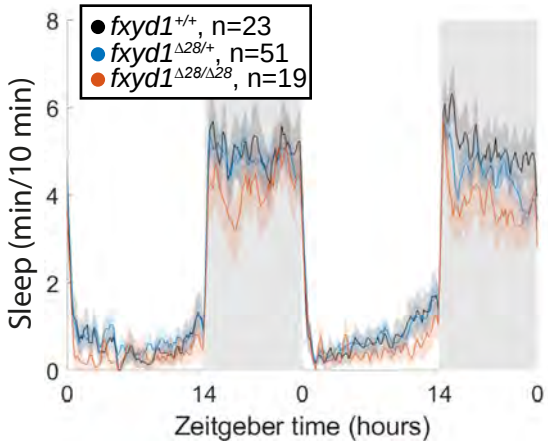

E)

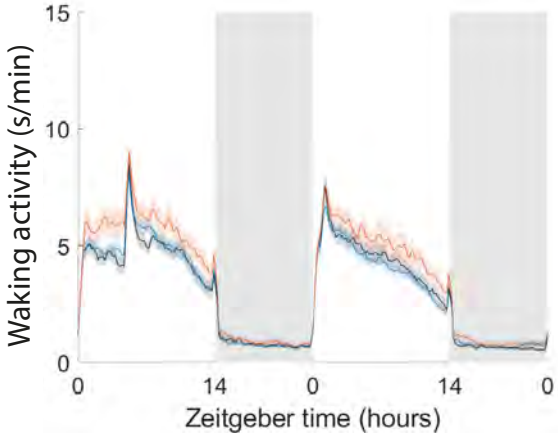

F)

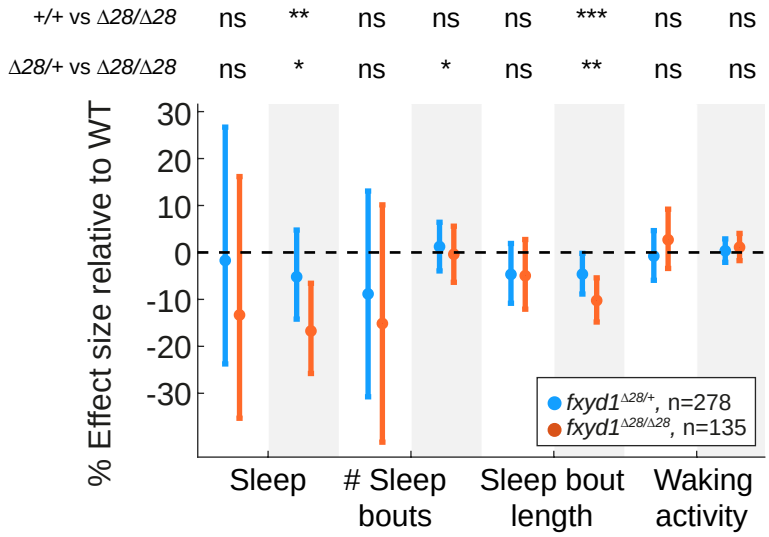

Figure 4

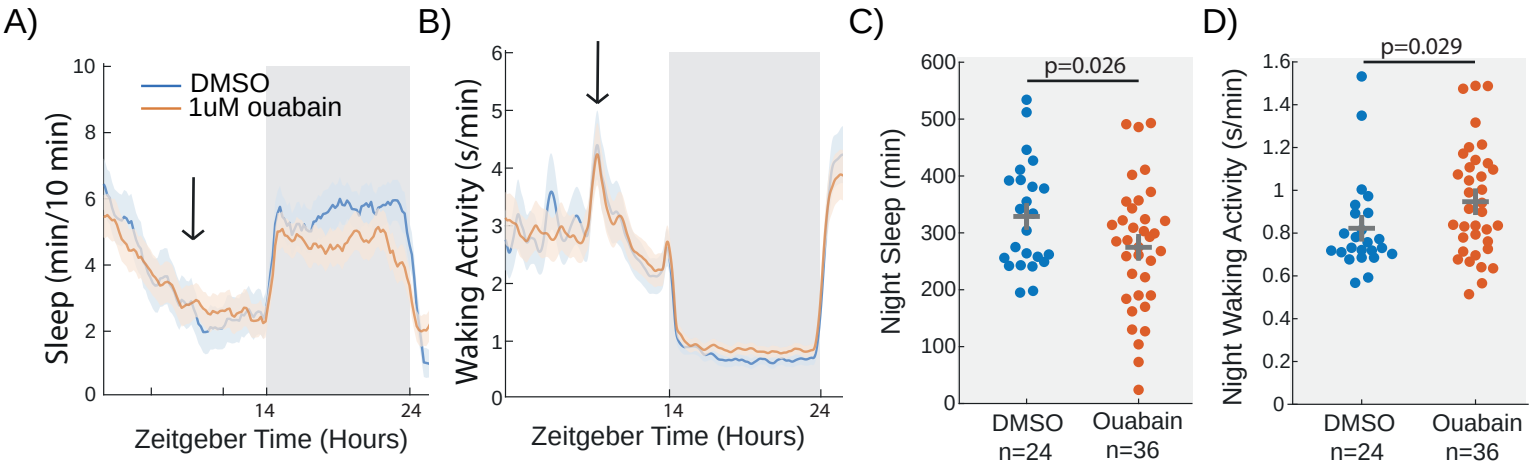
A)
DMSO
1uM ouabain
Sleep (min/10 min)
Zeitgeber Time (Hours)
B)
Waking Activity (s/min)
Zeitgeber Time (Hours)
C)
p=0.026
Night Sleep (min)
DMSO n=24
Ouabain n=36
D)
p=0.029
Night Waking Activity (s/min)
DMSO n=24
Ouabain n=36

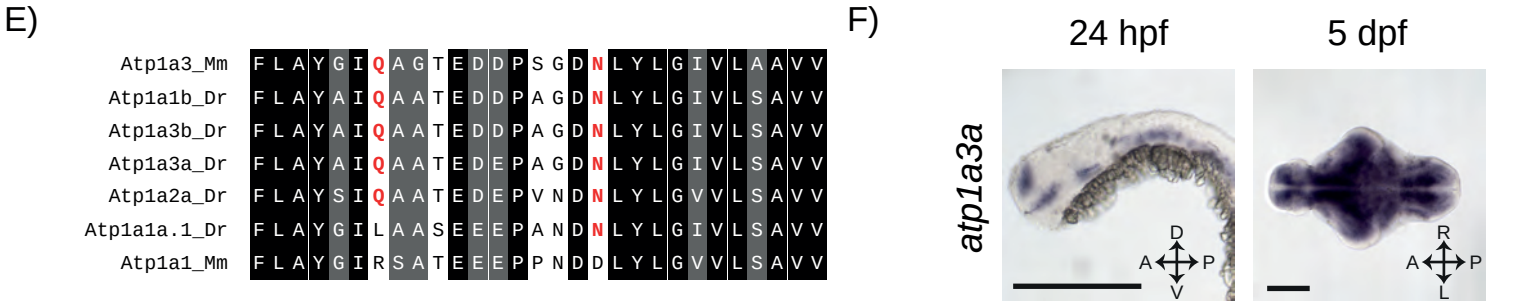
E)
Atp1a3_Mm
Atp1a1b_Dr
Atp1a3b_Dr
Atp1a3a_Dr
Atp1a2a_Dr
Atp1a1a.1_Dr
Atp1a1_Mm
F)
24 hpf
5 dpf
atp1a3a

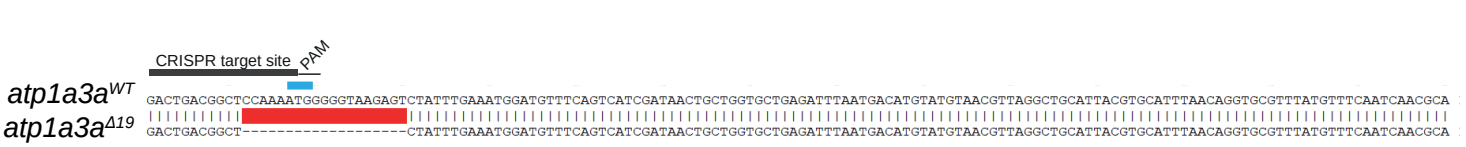
G)
CRISPR target site
PAM
atp1a3a^WT
atp1a3a^Δ19

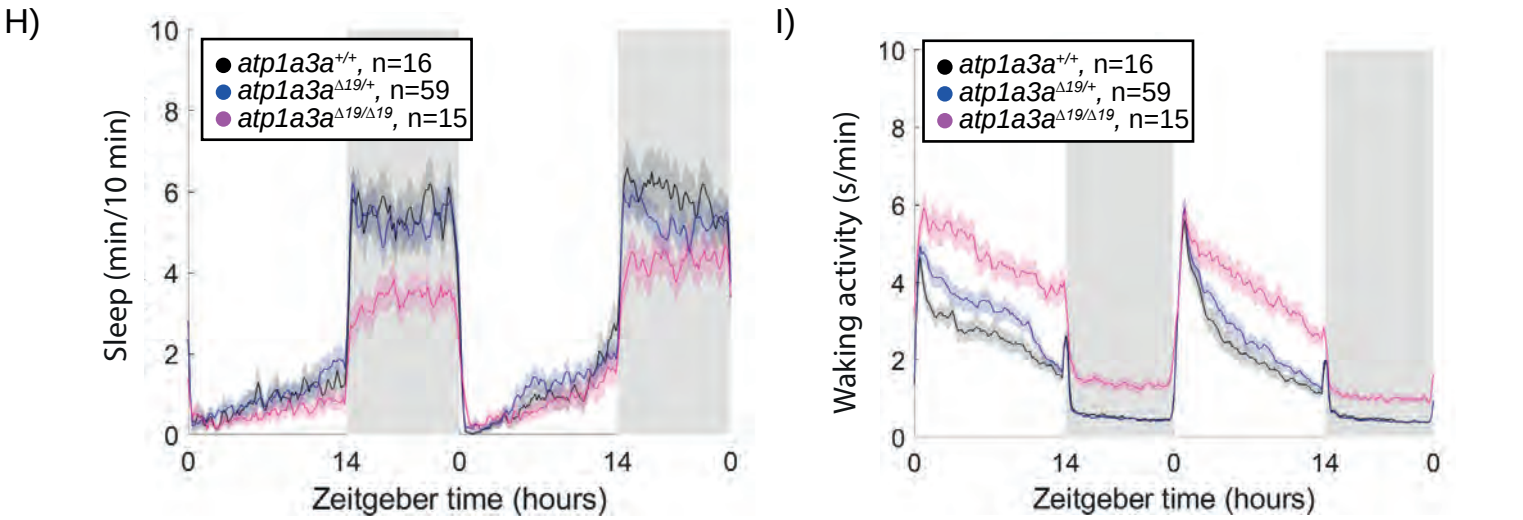
H)
atp1a3a+/+, n=16
atp1a3aΔ19/+, n=59
atp1a3aΔ19/Δ19, n=15
Sleep (min/10 min)
Zeitgeber time (hours)
I)
atp1a3a+/+, n=16
atp1a3aΔ19/+, n=59
atp1a3aΔ19/Δ19, n=15
Waking activity (s/min)
Zeitgeber time (hours)

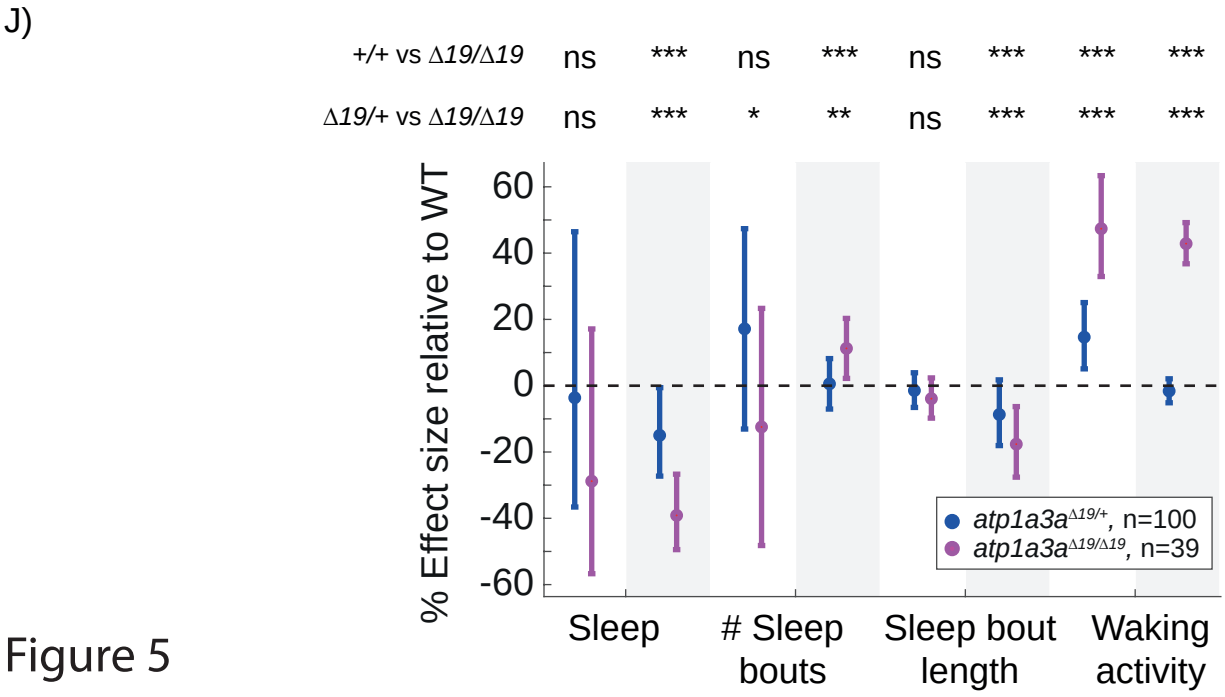
J)
+/+ vs Δ19/Δ19 ns *** ns *** ns *** *** ***
Δ19/+ vs Δ19/Δ19 ns *** * ** ns *** *** ***
% Effect size relative to WT
atp1a3aΔ19/+, n=100
atp1a3aΔ19/Δ19, n=39
Sleep
Sleep bouts
Sleep bout length
Waking activity

Figure 5

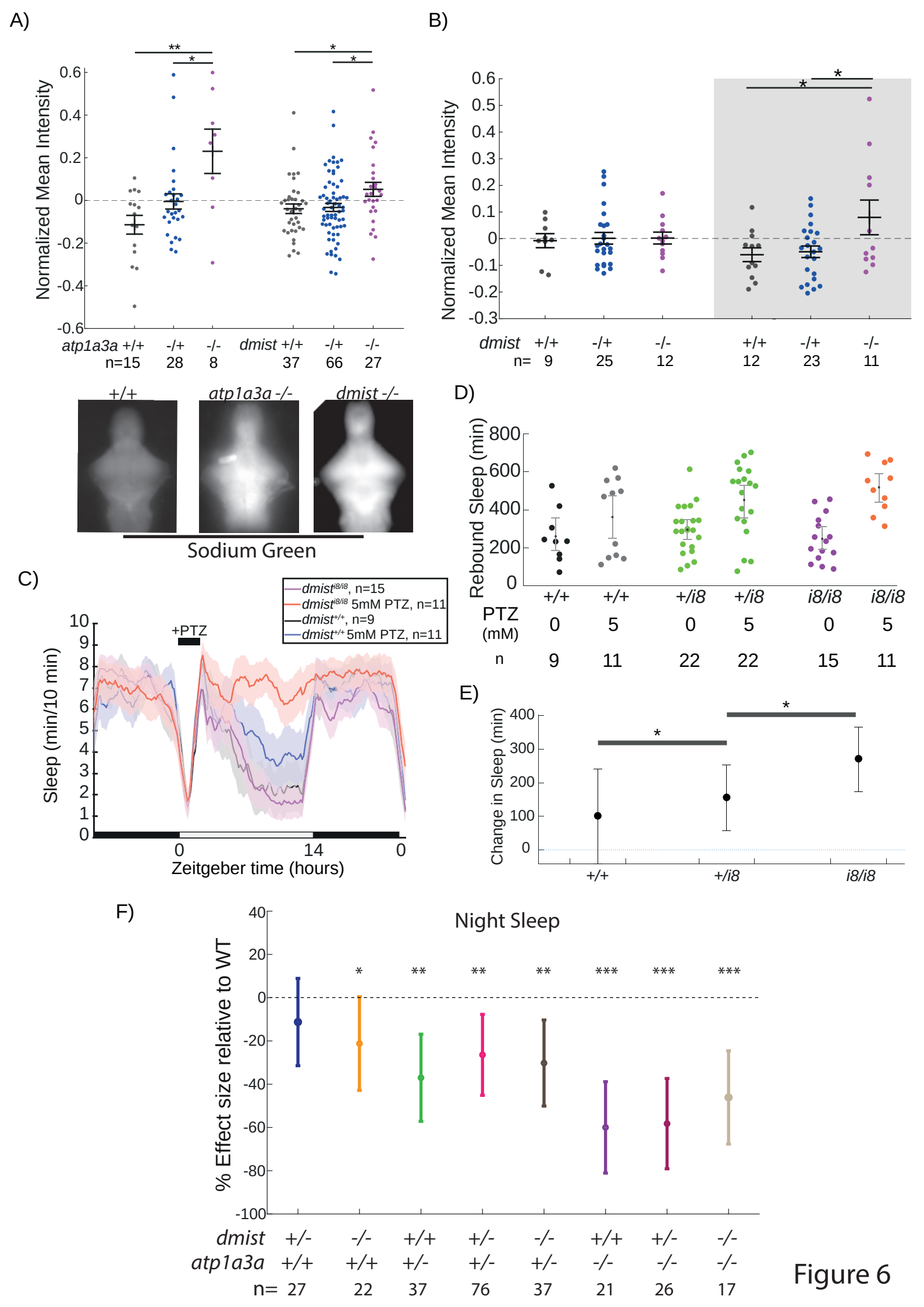
A)
Normalized Mean Intensity
atp1a3a +/+ -/+ -/- dmist +/+ -/+ -/-
n=15 28 8 37 66 27
B)
Normalized Mean Intensity
dmist +/+ -/+ -/- +/+ -/+ -/-
n= 9 25 12 12 23 11
+/+
atp1a3a -/-
dmist -/-
Sodium Green
C)
dmist i8/i8, n=15
dmist i8/i8 5mM PTZ, n=11
dmist +/+, n=9
dmist +/+ 5mM PTZ, n=11
+PTZ
Sleep (min/10 min)
Zeitgeber time (hours)
D)
Rebound Sleep (min)
+/+ +/+ +/i8 +/i8 i8/i8 i8/i8
PTZ (mM) 0 5 0 5 0 5
n 9 11 22 22 15 11
E)
Change in Sleep (min)
+/+ +/i8 i8/i8
F)
Night Sleep
% Effect size relative to WT
dmist +/- -/- +/+ +/- -/- +/+ +/- -/-
atp1a3a +/+ +/+ +/- +/- +/- -/- -/- -/-
n= 27 22 37 76 37 21 26 17

Figure 6

Figure S1

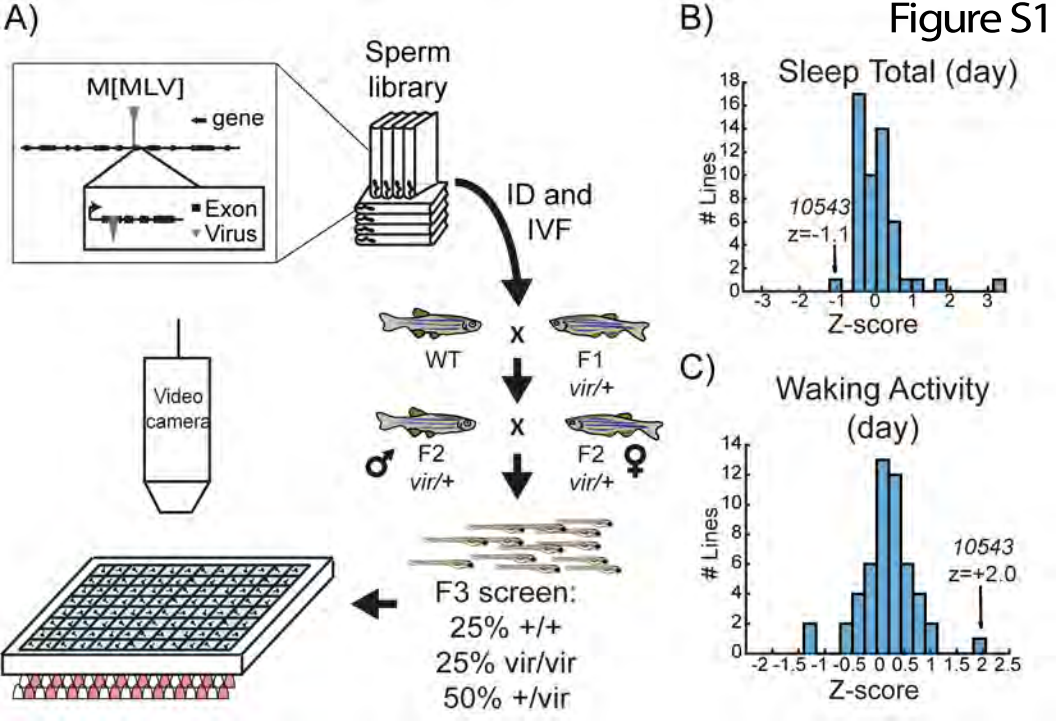
A)
M[MLV]
gene
Exon
Virus
Sperm library
ID and IVF
WT
F1
vir/+
x
F2
vir/+
F2
vir/+
Video camera
F3 screen:
25% +/+
25% vir/vir
50% +/vir
B)
Sleep Total (day)
Lines
10543
z=-1.1
Z-score
C)
Waking Activity (day)
Lines
10543
z=+2.0
Z-score

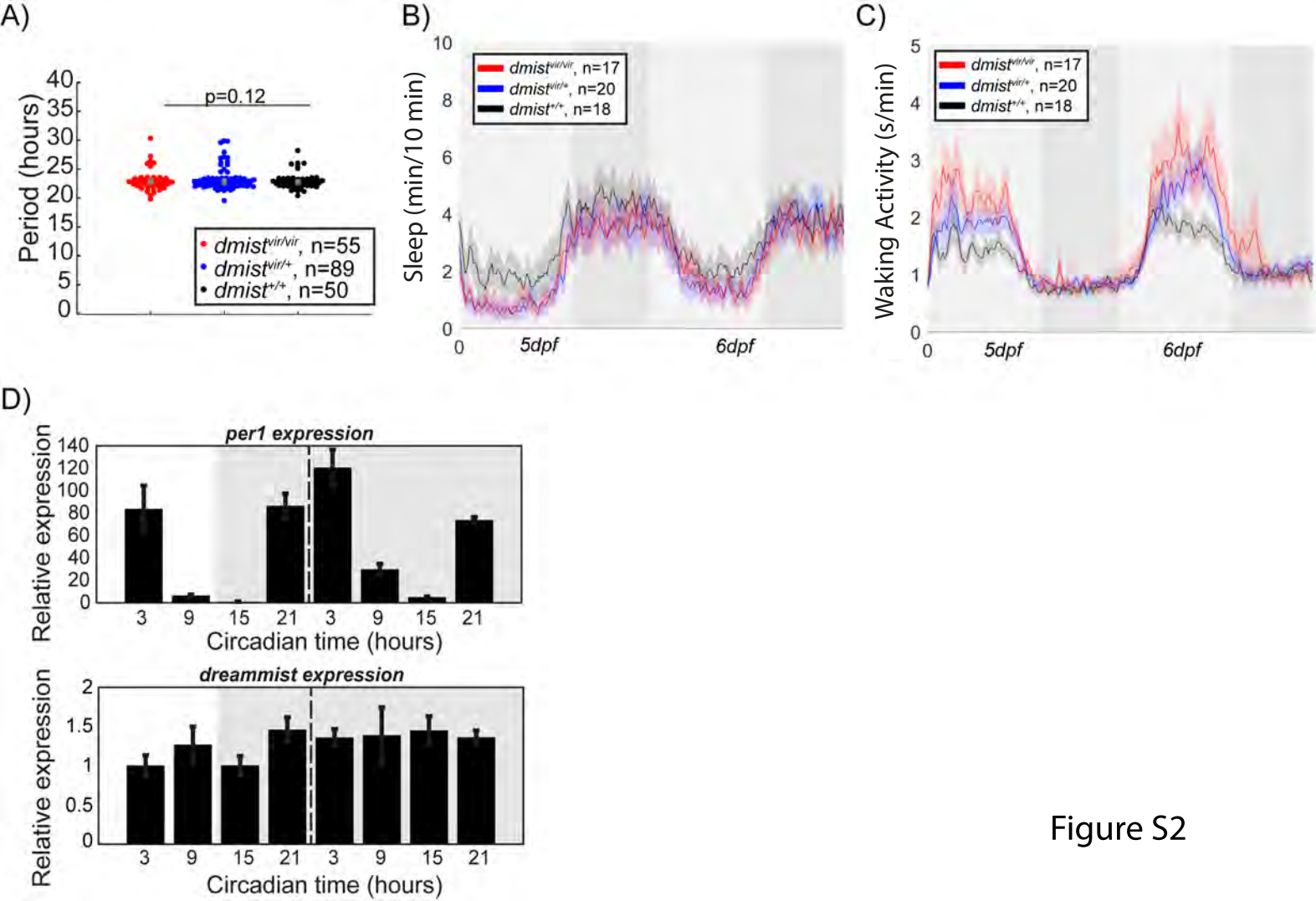
A)
Period (hours)
p=0.12
dmist vir/vir, n=55
dmist vir/+, n=89
dmist +/+, n=50
B)
Sleep (min/10 min)
dmist vir/vir, n=17
dmist vir/+, n=20
dmist +/+, n=18
5dpf
6dpf
C)
Waking Activity (s/min)
dmist vir/vir, n=17
dmist vir/+, n=20
dmist +/+, n=18
5dpf
6dpf
D)
per1 expression
Relative expression
Circadian time (hours)
dreammist expression
Relative expression
Circadian time (hours)

Figure S2

Figure S3

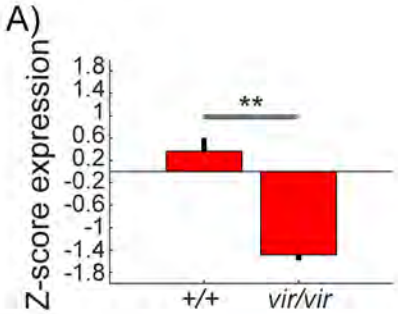

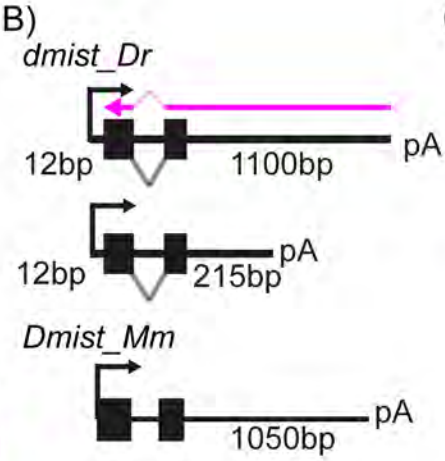

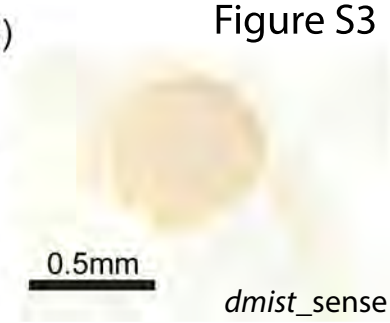

D)

Species	Danio rerio	Takifugu rupibes	Xenopus laevis	Gallus gallus	Mus musculus	Homo sapiens
Danio rerio	100.00	56.82	52.08	61.36	43.75	47.92
Takifugu rupibes	56.82	100.00	52.27	54.55	38.64	45.45
Xenopus laevis	52.08	52.27	100.00	68.18	46.00	52.00
Gallus gallus	61.36	54.55	68.18	100.00	65.91	72.73
Mus musculus	43.75	38.64	46.00	65.91	100.00	84.31
Homo sapiens	47.92	45.45	52.00	72.73	84.31	100.00

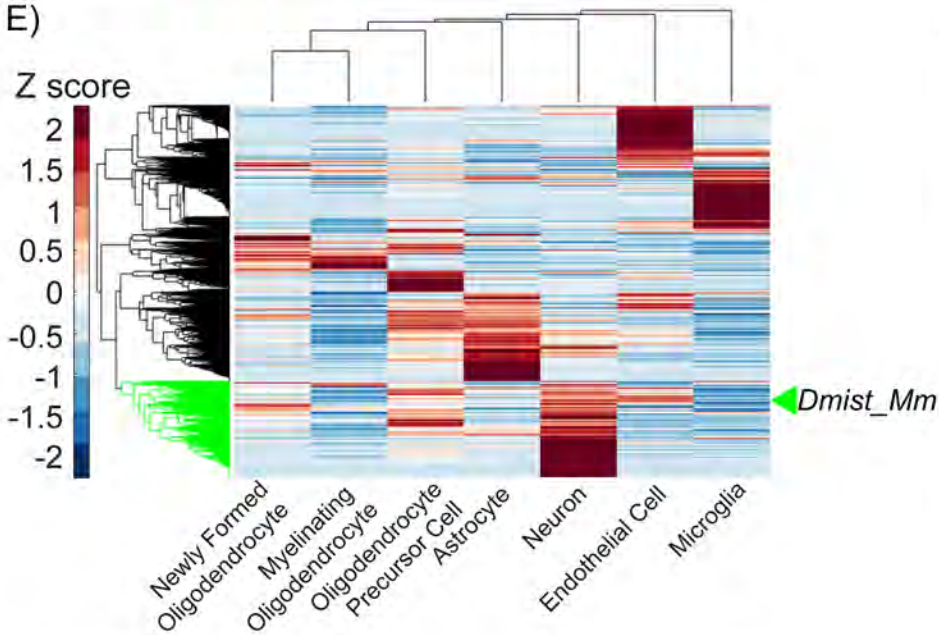

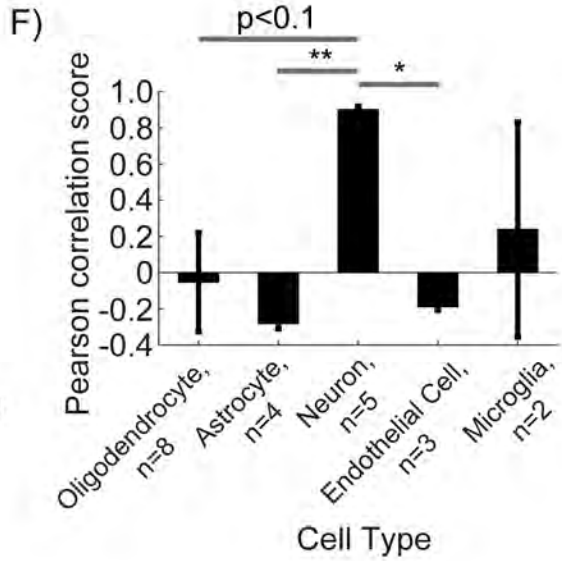

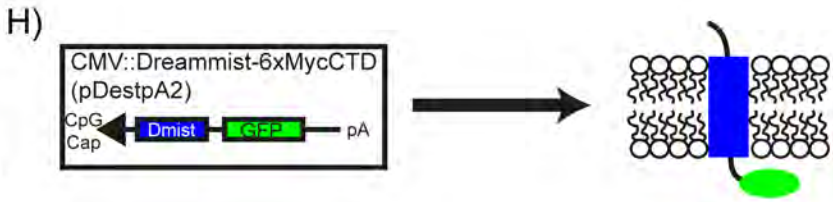

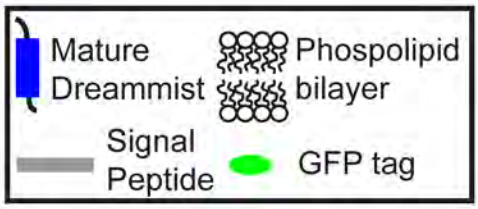

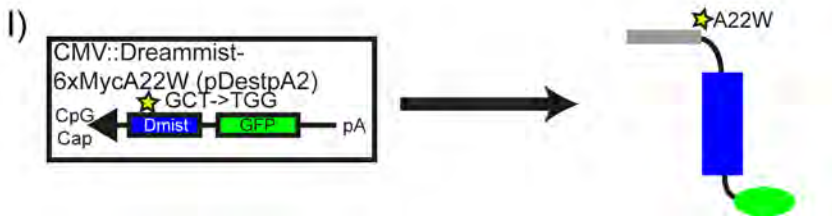

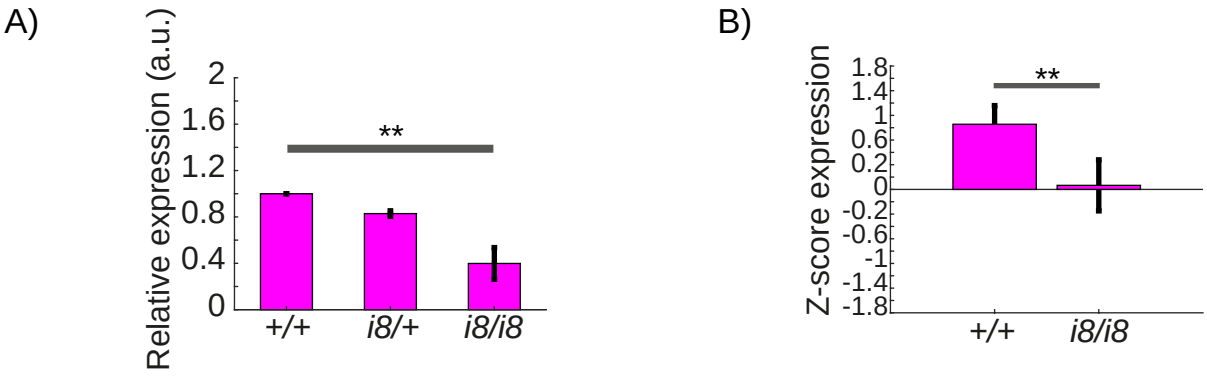
A)
Relative expression (a.u.)
2
1.6
1.2
0.8
0.4
0
**
+/+
i8/+
i8/i8
B)
Z-score expression
1.8
1.4
1
0.6
0.2
0
-0.2
-0.6
-1
-1.4
-1.8
**
+/+
i8/i8

Figure S4

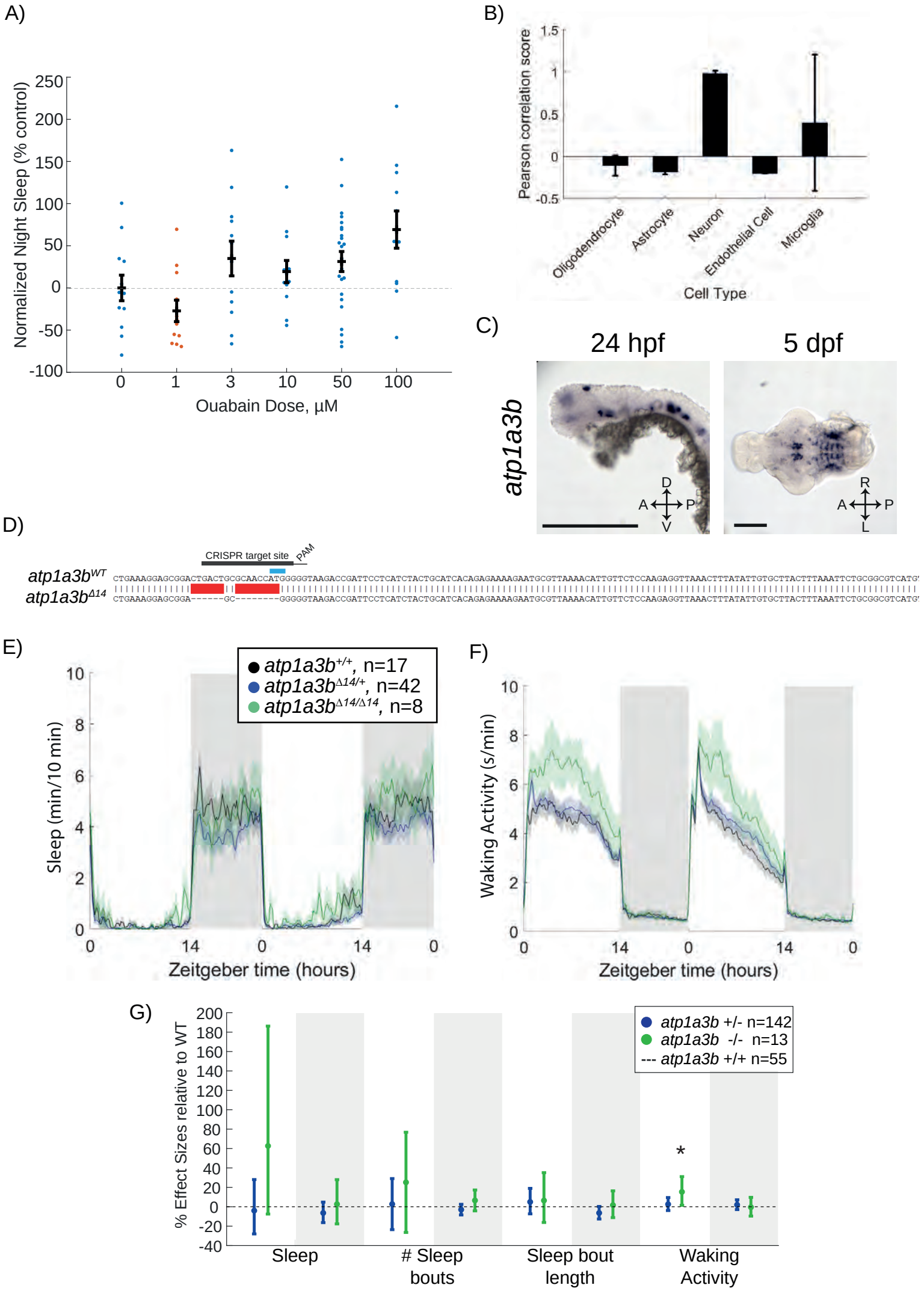
A)
Normalized Night Sleep (% control)
250
200
150
100
50
0
-50
-100
0
1
3
10
50
100
Ouabain Dose, µM
B)
Pearson correlation score
1.5
1
0.5
0
-0.5
Oligodendrocyte
Astrocyte
Neuron
Endothelial Cell
Microglia
Cell Type
C)
24 hpf
5 dpf
atp1a3b
D
A
P
V
R
A
P
L
D)
CRISPR target site
PAM
atp1a3b^WT
atp1a3b^Δ14
E)
atp1a3b+/+, n=17
atp1a3b^Δ14/+, n=42
atp1a3b^Δ14/Δ14, n=8
Sleep (min/10 min)
Zeitgeber time (hours)
F)
Waking Activity (s/min)
Zeitgeber time (hours)
G)
% Effect Sizes relative to WT
atp1a3b +/- n=142
atp1a3b -/- n=13
atp1a3b +/+ n=55
*
Sleep
Sleep bouts
Sleep bout length
Waking Activity

Figure S5

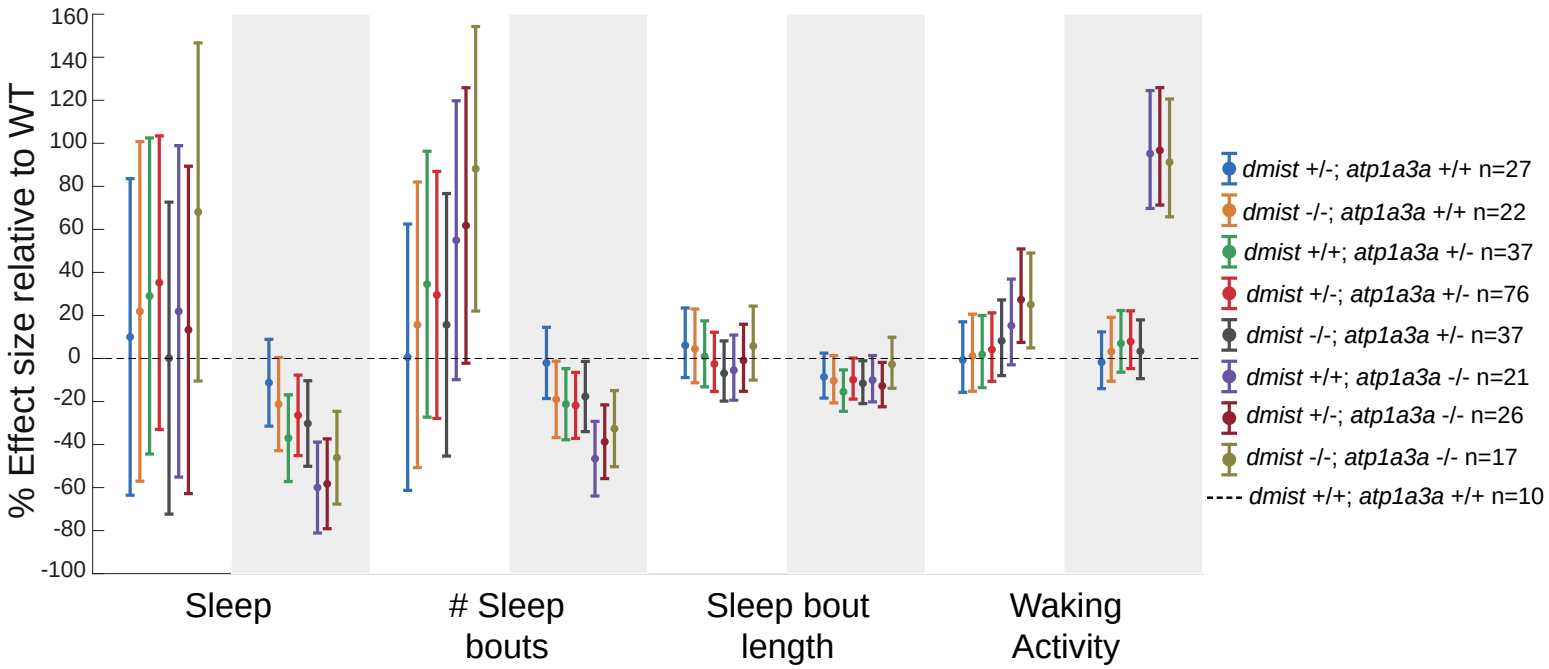
% Effect size relative to WT
160
140
120
100
80
60
40
20
0
-20
-40
-60
-80
-100
Sleep
Sleep bouts
Sleep bout length
Waking Activity
dmist +/-; atp1a3a +/+ n=27
dmist -/-; atp1a3a +/+ n=22
dmist +/+; atp1a3a +/- n=37
dmist +/-; atp1a3a +/- n=76
dmist -/-; atp1a3a +/- n=37
dmist +/+; atp1a3a -/- n=21
dmist +/-; atp1a3a -/- n=26
dmist -/-; atp1a3a -/- n=17
dmist +/+; atp1a3a +/+ n=10

Figure S6